Dalton Transactions

RSC Publishing

PAPER

View Article Online
View Journal | View Issue

Cite this: *Dalton Trans.*, 2013, **42**, 6538

9,10-Phenanthrenesemiquinone radical complexes of ruthenium(III), osmium(III) and rhodium(III) and redox series†

Manas Kumar Biswas,[a] Sarat Chandra Patra,[a] Amarendra Nath Maity,[b] Shyue-Chu Ke,[b] Thomas Weyhermüller[c] and Prasanta Ghosh*[a]

Reactions of 9,10-phenanthrenequinone (PQ) in toluene with [$M^{II}(PPh_3)_3X_2$] at 298 K afford green complexes, *trans*-[$M(PQ)(PPh_3)_2X_2$] (M = Ru, X = Cl, **1**; M = Os, X = Br, **2**) in moderate yields. Reaction of anhydrous $RhCl_3$ with PQ and PPh_3 in boiling ethanol affords the dark brown paramagnetic complex, *cis*-[$Rh(PQ)(PPh_3)_2Cl_2$] (**3**) in good yields. Diffusion of iodine solution in *n*-hexane to the *trans*-[$Os(PQ)(PPh_3)_2(CO)(Br)$] solution in CH_2Cl_2 generates the crystals of *trans*-[$Os(PQ)(PPh_3)_2(CO)(Br)]^+I_3^-$, ($\mathbf{4}^+I_3^-$), in lower yields. Single crystal X-ray structure determinations of **1**·2toluene, **2**·CH_2Cl_2 and $\mathbf{4}^+I_3^-$, UV-vis/NIR absorption spectra, EPR spectra of **3**, electrochemical activities and DFT calculations on **1**, **2**, *trans*-[$Ru(PQ)(PMe_3)_2Cl_2$] ($\mathbf{1}_{Me}$), *trans*-[$Os(PQ)(PMe_3)_2Br_2$] ($\mathbf{2}_{Me}$), *cis*-[$Rh(PQ)(PMe_3)_2Cl_2$] ($\mathbf{3}_{Me}$) and their oxidized and reduced analogues including *trans*-[$Os(PQ)(PMe_3)_2(CO)(Br)]^+$ ($\mathbf{4}_{Me}^+$) substantiated that **1**–**3** are the 9,10-phenanthrenesemiquinone radical ($PQ^{\cdot-}$) complexes of ruthenium(III), osmium(III) and rhodium(III) and are defined as *trans*/*cis*-[$M^{III}(PQ^{\cdot-})(PPh_3)_2X_2$] with a minor contribution of the resonance form *trans*/*cis*-[$M^{II}(PQ)(PPh_3)_2X_2$]. Two comparatively longer C–O (1.286(4) Å) and the shorter C–C lengths (1.415(7) Å) of the OO-chelate of **1**·2toluene and **2**·CH_2Cl_2 and the isotropic fluid solution EPR signal at g = 1.999 of **3** are consistent with the existence of the reduced $PQ^{\cdot-}$ ligand in **1**–**3** complexes. Anisotropic EPR spectra of the frozen glasses ($g_{11} = g_{22}$ = 2.0046 and g_{33} = 1.9874) and solids ($g_{11} = g_{22}$ = 2.005 and g_{33} = 1.987) instigate the contribution of the resonance form, *cis*-[$Rh^{II}(PQ)(PPh_3)_2Cl_2$] in **3**. DFT calculations established that the closed shell singlet (CSS) solutions of $\mathbf{1}_{Me}$ and $\mathbf{2}_{Me}$ are unstable due to open shell singlet (OSS) perturbation. However, the broken symmetry (BS) (1,1) M_s = 0 solutions of $\mathbf{1}_{Me}$ and $\mathbf{2}_{Me}$ are respectively 22.6 and 24.2 kJ mole^{-1} lower in energy and reproduced the experimental bond parameters well prompting the coordination of $PQ^{\cdot-}$ to the M(III) ions. The comparatively shorter C–O lengths, 1.268(4) and 1.266(5) Å and the longer C–C length, 1.466(6) Å, are consistent with the PQ chelation to osmium(II) ion in $\mathbf{4}^+$. The reversible anodic waves at 0.22, 0.22, and 0.18 V of **1**–**3**, referenced by the Fc^+/Fc couple, are assigned to the $PQ^{\cdot-}$/PQ couple forming PQ complexes as *trans*/*cis*-[$M^{III}(PQ)(PPh_3)_2X_2]^+$ while the cathodic waves at −0.92 and −0.89 V of **2** and **3** are due to formations of PQ^{2-} complexes as *trans*-[$M^{III}(PQ^{2-})(PPh_3)_2X_2]^-$. **1** displays two overlapping cathodic waves at −0.72(89), −1.0(120) V. EPR spectrum of the frozen glass of $\mathbf{1}^-$ along with DFT calculations detected the contribution of both the valence tautomers, *trans*-[$Ru^{III}(PQ^{2-})(PPh_3)_2Cl_2]^-$ ($g_1 = g_2$ = 2.456; g_3 = 1.983) and *trans*-[$Ru^{II}(PQ^{\cdot-})(PPh_3)_2X_2]^-$ (g_{iso} = 1.999) in the anion. The characteristic lower energy absorption bands of **1** and **2** at 700 nm were assigned to CSS–OSS perturbation MLCT those are absent in paramagnetic **3**, $\mathbf{1}^+$, $\mathbf{2}^+$, $\mathbf{1}^-$, $\mathbf{2}^-$ and $\mathbf{4}^+$ complexes, investigated by spectro-electrochemical measurements and time dependent (TD) DFT calculations on $\mathbf{1}_{Me}$, $\mathbf{2}_{Me}$, $\mathbf{1}_{Me}^+$ and $\mathbf{1}_{Me}^-$.

Received 4th January 2013,
Accepted 12th February 2013

DOI: 10.1039/c3dt00038a

www.rsc.org/dalton

[a] *Department of Chemistry, R. K. Mission Residential College, Narendrapur, Kolkata-103, India. E-mail: ghosh@pghosh.in; Fax: +91 33 2477 3597; Tel: +91 33 2428 7347*

[b] *Department of Physics, National Dong Hwa University, Shou-Feng, Hualien 97401, Taiwan*

[c] *Max-Planck Institute for Chemical Energy Conversion, 45470 Muelheiman der Ruhr, Germany*

†Electronic supplementary information (ESI) available: X-ray crystallographic CIF files of **1**·2toluene, **2**·CH_2Cl_2 and $\mathbf{4}^+I_3^-$, EPR parameters (Table S1), redox potentials (Table S2), optimized geometries (Fig. S1) and optimized coordinates (Tables S3–S13). CCDC 917746–917748. For ESI and crystallographic data in CIF or other electronic format see DOI: 10.1039/c3dt00038a

Introduction

Precise definition of the electronic states of the coordination complexes incorporating two or more redox active sites is significant to predict the relevant electron transfer sites in a complex bio-molecule.[1] In this context several redox active molecules parallel to bio-molecules were reported.[2] Elucidation of the electronic structures of the complexes incorporating redox active metal ions and the redox active ligand is a subject of investigation in chemistry. 9,10-Phenanthrenequinone (PQ) is redox active and a biologically hazardous molecule that undergoes one electron reduction to the 9,10-phenanthrenesemiquinone radical ($PQ^{\cdot-}$) at lower potential.[3] Recently, the electronic structures of a paramagnetic family of PQ of type *trans*-[M(PQ)(PPh_3)$_2$(CO)(X)] and *cis*-[M(PQ)(PPh_3)$_2$(CO)(X)] with the redox-active metal ions (M = Ru, Os; X = Cl, Br) incorporating triphenyl phosphine (PPh_3), carbonyl and halide as co-ligands were reported.[4] The article disclosed that *trans*-[M(PQ)(PPh_3)$_2$(CO)(X)] and *cis*-[M(PQ)(PPh_3)$_2$(CO)(X)] are $PQ^{\cdot-}$ complexes of ruthenium(II) and osmium(II), as shown by **A**, defined as *trans*-[M^{II}($PQ^{\cdot-}$)(PPh_3)$_2$(CO)X] and *cis*-[M^{II}($PQ^{\cdot-}$)-(PPh_3)$_2$(CO)X] with a minor contribution of the alternate resonance form, *trans* or *cis*-[M^{I}(PQ)(PPh_3)$_2$(CO)X], as illustrated by **B** of Scheme 1. Significant observations documented in the article are: (i) all the anionic complexes are PQ^{2-} complexes of ruthenium(II)/osmium(II) (ii) all the cationic complexes are neutral PQ complexes of ruthenium(II)/osmium(II) (iii) the ground state electronic structure of the neutral paramagnetic complexes is best described by a superposition of the valence tautomers of $PQ^{\cdot-}$ coordinated to ruthenium(II)/osmium(II) and PQ coordinated to ruthenium(I)/osmium(I) ions and (iv) $PQ^{\cdot-}/PQ^{2-}$ redox couple of the *cis*-analogues is irreversible even at 253 K due to the PPh_3 dissociation.

In 1975 a diamagnetic PQ complex of ruthenium incorporating PPh_3 and Cl as coligands, [Ru(PQ)(PPh_3)$_2$$Cl_2$] (**1**) was reported.[5] **1** was predicted as a 9,10-phenanthrenediolato complex of ruthenium(IV) as depicted by the resonance form **C** of Scheme 2. However, it contradicts the coexistence of a highly oxidizing ruthenium(IV) ion coordinated to an easily oxidizable 9,10-phenanthrenediolato di-anion and we have been persuaded to disclose the electronic structures of the *trans*/*cis*-[M(PQ)(PPh_3)$_2$$X_2$] (M = Ru, X = Cl, **1**; M = Os, X = Br, **2**; M = Rh, X = Cl, **3**) family incorporating PPh_3 and halide as coligands. A complete experimental and theoretical investigation completely denied the existence of the metal(IV) ion coordinated to 9,10-phenanthrenediolato di-anion (PQ^{2-}) in **1–3**, rather the

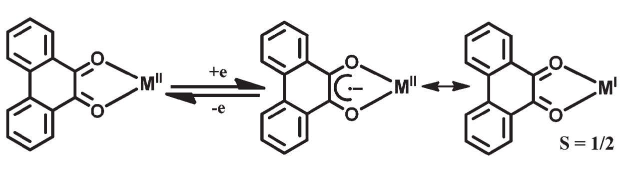

[M^{II}(PQ)] [M^{II}($PQ^{\bullet-}$)] (A) [M^{I}(PQ)] (B)

Scheme 1

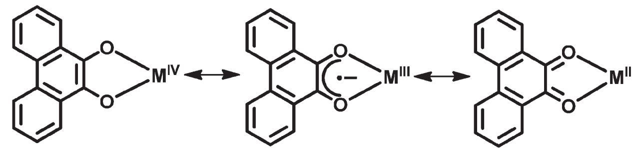

[M^{IV}(PQ^{2-})] (C) [M^{III}($PQ^{\bullet-}$)] (D) [M^{II}(PQ)] (E)

Scheme 2

trans-[Ru(PQ)(PMe_3)$_2$$Cl_2$]	$\mathbf{1}_{Me}$	corresponds to	**1**
trans-[Os(PQ)(PMe_3)$_2$$Br_2$]	$\mathbf{2}_{Me}$	corresponds to	**2**
cis-[Rh(PQ)(PMe_3)$_2$$Cl_2$]	$\mathbf{3}_{Me}$	corresponds to	**3**
trans-[Os(PQ)(PMe_3)$_2$(CO)(Br)]$^+$	$\mathbf{4}_{Me}^+$	corresponds to	$\mathbf{4}^+$

Chart 1 Model complexes of **1–3** and $\mathbf{4}^+$ used for DFT calculations.

study authenticated the coordination of $PQ^{\cdot-}$ to the ruthenium(III), osmium(III) and rhodium(III) ions in **1–3** as described by the resonance form **D** of Scheme 2. Moreover, a minor contribution of the bivalent metal ion coordinated to the 9,10-phenanthrenequinone as illustrated by the resonance form **E** (Scheme 2) to the ground electronic state of **1–3** complexes has been detected. On the contrary, the single crystal X-ray bond parameters and DFT calculations attested that *trans*-[Os(PQ)-(PPh_3)$_2$(CO)(Br)]$^+$$I_3^-$, $\mathbf{4}^+I_3^-$ is a pure PQ complex and the electronic state of the $\mathbf{4}^+$ cation has been precisely described by the resonance form **E** only. The electrogenerated $[\mathbf{1}\text{–}\mathbf{3}]^+$ ions are authenticated as PQ complexes of M(III) ions while $[\mathbf{2}\text{–}\mathbf{3}]^-$ are the PQ^{2-} complexes of M(III) ions. $\mathbf{1}^-$ is composed of two valence tautomers,[6] [Ru^{III}(PQ^{2-})] ↔ [Ru^{II}($PQ^{\cdot-}$)], confirming the existence of the $PQ^{\cdot-}$ anion radical coordinated to the metal(III) ion in **1–3** complexes. The molecular and electronic structures of the complexes reported in this article are analyzed by the single crystal X-ray structure determinations, UV-vis/NIR and EPR spectra, redox series and broken symmetry (BS) and time dependent (TD) DFT calculations on **1**, **2** and on the corresponding model complexes, $\mathbf{1}_{Me}$, $\mathbf{2}_{Me}$, $\mathbf{3}_{Me}$ and $\mathbf{4}_{Me}^+$ as listed in Chart 1.

Experimental section

Materials

Reagents or analytical grade materials were obtained from commercial suppliers and used without further purification. Spectroscopic grade solvents were used for spectroscopic and electrochemical measurements. The precursors [$RuCl_2$-(PPh_3)$_3$],[7] [$OsBr_2$(PPh_3)$_2$],[8] *trans*-[Os(PQ)(PPh_3)$_2$(CO)Br] (**4**)[4] were prepared by the reported procedures. The physicochemical data were collected on the isolated *trans*-[Ru(PQ)-(PPh_3)$_2$$Cl_2$] (**1**), *trans*-[Os(PQ)(PPh_3)$_2$$Br_2$] (**2**), *cis*-[Rh(PQ)-(PPh_3)$_2$$Cl_2$] (**3**) and *trans*-[Os(PQ)(PPh_3)$_2$(CO)(Br)]$^+$$I_3^-$ ($\mathbf{4}^+I_3^-$) complexes. However, theoretical calculations were performed on **1**, **2** and corresponding model complexes which incorporate PMe_3 ligands as listed in Chart 1.

Syntheses

***trans*-[Ru(PQ)(PPh$_3$)$_2$Cl$_2$] (1).** **1** was first prepared by Balch *et al.*[5] However, **1** was synthesized here by a different procedure and characterized with Mass, ^{1}H NMR and IR spectra. To a saturated solution of PQ in toluene (40 ml) [Ru^{II}(PPh$_3$)$_3$Cl$_2$] (100 mg, 0.10 mmol) in toluene (20 ml) was added under argon and the solution was stirred at room temperature for 1 h. A dark green solid of **1** separated out, which was filtered, dried in air and collected. Yield: 70 mg (74% with respect to ruthenium). Single crystals for X-ray analyses were prepared by diffusion of a saturated solution of PQ in toluene (50 ml) to a solution of [Ru^{II}(PPh$_3$)$_3$Cl$_2$] (50 mg, 0.05 mmol) in chlorobenzene (10 ml) in a stoppered glass tube at room temperature (298 K). Within one or two days, the junction of the two layers turned green depositing dark green crystals on the glass wall. It was allowed to diffuse for another 15 days, while dark green crystals of **1**·2toluene separated in both layers which are collected upon filtration and dried in air. Mass spectral data [electrospray ionization (ESI) positive ion, CH$_2$Cl$_2$]: *m*/*z* 927.03 for [**3** + Na]$^+$. Anal. Calcd for C$_{64}$H$_{54}$Cl$_2$O$_2$P$_2$Ru: C, 70.58; H, 5.00. Found: C, 70.02; H, 4.70. ^{1}H NMR (CDCl$_3$, 300 MHz): δ 8.28 (d, H), 8.10 (d, H), 8.02 (t, H), 7.66 (d, 2H), 7.64 (t, H), 7.54 (m, PPh$_3$), 7.39 (t, 2H), 7.17 (m, PPh$_3$). ^{1}H NMR (DMSO-d$_6$, 300 MHz): δ 8.32 (d, H), 8.04 (d, H), 7.80 (t, H), 7.64 (d, 2H), 7.54 (t, 2H), 7.40 (m, PPh$_3$), 7.24 (m, PPh$_3$), 7.19 (t, H). IR/cm^{-1} (KBr): ν 1632 (vs), 1458 (m, $\nu_{C=O(sym)}$), 1435 (m, $\nu_{C=O(asym)}$), 1388 (m), 1350 (s), 1096 (m), 694 (s, $\nu_{Ru-P(sym)}$), 519 (s, $\nu_{Ru-P(asym)}$).

***trans*-[Os(PQ)(PPh$_3$)$_2$Br$_2$] (2).** To a saturated solution of PQ in toluene (40 ml) [Os^{II}(PPh$_3$)$_3$Br$_2$] (100 mg, 0.09 mmol) in toluene (20 ml) was added under argon and the solution was stirred at room temperature for 1 h. A dark green solid of **2** separated out, which was filtered, dried in air and collected. Yield: 60 mg (63% with respect to osmium). Single crystals as **2**·CH$_2$Cl$_2$ for X-ray analyses were prepared by slow diffusion of *n*-hexane to the CH$_2$Cl$_2$ solution of **2** in a glass tube at 298 K. Mass spectral data [electrospray ionization (ESI) positive ion, CH$_2$Cl$_2$]: *m*/*z* 1082.03 for [**2**]$^+$. Anal. Calcd for C$_{50}$H$_{38}$Br$_2$O$_2$P$_2$Os: C, 55.46; H, 3.54. Found: C, 55.03; H, 3.22. ^{1}H NMR (CDCl$_3$, 300 MHz): δ 8.22 (d, H), 8.06 (d, H), 8.00 (t, H), 7.59 (d, 2H), 7.63 (t, H), 7.44 (m, PPh$_3$), 7.38 (t, 2H), 7.07 (m, PPh$_3$). IR/cm^{-1} (KBr): ν 1654 (m), 1597 (m), 1558 (m), 1497 (m), 1480 (m), 1433 (s), 1399 (s), 1318 (s), 1094 (s), 745 (s) 693 (vs), 520 (vs).

***cis*-[Rh(PQ)(PPh$_3$)$_2$Cl$_2$] (3).** To a hot solution of 9,10-phenanthrenequinone (125 mg, 0.6 mmol) in absolute ethanol (30 ml), RhCl$_3$ (75 mg, 0.36 mmol) and PPh$_3$ (315 mg, 1.2 mmol) were added successively, and the reaction mixture was refluxed for 40 min at 351 K under argon atmosphere. A violet crystalline solid separated out. The solution mixture was cooled to room temperature and filtered. The residue was dried in vacuum and collected for further analyses. Yield: 280 mg (85% with respect to rhodium). Mass spectral data [electrospray ionization (ESI) positive ion, CH$_2$Cl$_2$]: *m*/*z* 908.42 [**3**], 874.40 [**3** − Cl]$^+$. Anal. Calcd for C$_{50}$H$_{38}$Cl$_2$O$_2$P$_2$Rh: C, 66.24; H, 4.22. Found: C, 65.98; H, 3.88. IR/cm^{-1} (KBr): ν 1595 (m), 1481 (s), 1432 (vs), 1376 (s), 1096 (s), 742 (s), 688 (vs), 520 (vs).

***trans*-[Os(PQ)(PPh$_3$)$_2$(CO)Br]$^+$I$_3^-$ (4$^+$I$_3^-$).** To a solution of *trans*-[Os(PQ)(PPh$_3$)$_2$(CO)Br] (**4**) (50 mg, 0.05 mmol) in CH$_2$Cl$_2$ (20 ml), I$_2$ (12 mg, 0.05 mmol) solution in *n*-hexane (20 ml) was allowed to diffuse at 298 K. After 4–5 days, black needles of **4**$^+$I$_3^-$ separated out, which were filtered and dried in air (single crystals for X-ray diffraction study were collected from this product). Yield: 5 mg (7.3% with respect to **4**). Mass spectral data [electrospray ionization (ESI) positive ion, CH$_2$Cl$_2$]: *m*/*z* 1032.2 for **4**$^+$. Anal. Calcd for C$_{51}$H$_{38}$BrO$_3$P$_2$OsI$_3$: C, 43.39; H, 2.71. Found: C, 42.78; H, 2.32. ^{1}H NMR (CDCl$_3$, 600 MHz): δ 8.21 (d, H), 8.03 (d, H), 7.73 (t, H), 7.67 (d, H), 7.66 (d, H), 7.55 (t, H), 7.48 (m, PPh$_3$), 7.38 (t, H), 7.32 (m, PPh$_3$), 7.19 (t, H). IR/cm^{-1} (KBr): ν 1955 (vs, $\nu_{C\equiv O}$), 1676 (s,$\nu_{c=c\ (PQ)}$), 1594 (s, $\nu_{c=o(asym)}$), 1560 (m, $\nu_{C=O(sym)}$), 1436, 1362, 1283, 1093 (m, $\nu_{PQ(skel)}$), 760 (m, $\nu_{C-H(wagg)}$), 694 (vs, $\nu_{Ru-P(sym)}$), 524 (vs, $\nu_{Ru-P(asym)}$).

Physical measurements

Commercially available spectroscopic grade solvents were used for spectroscopic and electrochemical measurements. The C and H content of the compounds were obtained from Perkin-Elmer 2400 series II elemental analyzer. Infrared spectra of the samples were measured from 4000 to 400 cm^{-1} with the KBr pellet at room temperature on a Perkin-Elmer Spectrum RX I, FT-IR spectrophotometer. ^{1}H NMR spectra were carried out on a Bruker Avance DPX-600 MHz and Bruker DPX-300 MHz spectrometers. ESI mass spectra were recorded on a micro mass Q-TOF mass spectrometer. Electronic absorption spectra in solution at 298 K were carried out on a Perkin-Elmer Lambda 25 spectrophotometer in the range of 1100–200 nm. The X-band electron paramagnetic resonance (EPR) spectra were measured on a Bruker EMX spectrometer, where the microwave frequency was measured with a Hewlett-Packard 5246L electronic counter. Q-band spectra were measured using Bruker EMX spectrometer with Microwave Frequency = 33.936 GHz, Power = 1.997 mW, Modulation amplitude = 2.00 G. Magnetic susceptibility at 298 K was measured on Sherwood Magnetic Susceptibility Balance. The electro analytical instrument, BASi Epsilon-EC for cyclic voltammetric experiment in CH$_2$Cl$_2$ solution containing 0.2 M tetrabutylammonium hexafluorophosphate as supporting electrolyte was used. The BASi platinum working electrode, platinum auxiliary electrode, Ag/AgCl reference electrode were used for the measurements. The redox potential data are referenced *vs.* ferrocenium/ferrocene, Fc$^+$/Fc, couple. In all cases, the experiments were performed with multiple scan rates to analyse the reversibility of the electron transfer waves. BASi SEC-C thin layer quartz glass spectroelectrochemical cell kit (light path length of 1 mm) with platinum gauze working electrode and SEC-C platinum counter electrode were used for spectroelectrochemical measurements.

X-ray crystallographic data collections and refinement of the structures (CCDC 917746–917748)†

Thin crystals of **1**·2toluene, **2**·CH$_2$Cl$_2$ and **4**$^+$I$_3^-$ were picked up with the nylon loops and were mounted on a Bruker Kappa-

Table 1 Crystallographic data for **1**·2toluene, **2**·CH_2Cl_2 and $\mathbf{4}^+I_3^-$

	1·2toluene	**2**·CH_2Cl_2	$\mathbf{4}^+I_3^-$
Formula	$C_{64}H_{54}Cl_2O_2P_2Ru$	$C_{51}H_{40}Br_2Cl_2O_2P_2Os$	$C_{51}H_{38}BrI_3O_3P_2Os$
Fw	1088.98	1167.69	1411.56
Crystal colour	Dark green	Dark green	Black
Crystal system	Monoclinic	Monoclinic	Monoclinic
Space group	$C2/c$	$C2/c$	$P2_1/c$
a (Å)	31.372(2)	23.5613(9)	13.243(2)
b (Å)	11.467(1)	11.6716(14)	14.0856(12)
c (Å)	17.589(1)	17.879(2)	25.252(4)
β (°)	123.500(3)	116.797(7)	90.390(11)
V (Å^3)	5276.6(4)	4388.7(7)	4710.3(11)
Z	4	4	4
T (K)	293 (2)	100 (2)	100 (2)
Calcd (g cm^{-3})	1.371	1.767	1.991
Reflns collected	19 262	40 373	79 466
Unique reflns	4474	8269	15 661
Reflns [$I > 2\sigma(I)$]	3836	7688	12 787
λ (Å)/μ (mm^{-1})	0.71073/0.504	0.71073/4.963	0.71073/5.632
F(000)	2248	2288	2672
$R_1{}^a$ [$I > \sigma(I)$]/GOF^b	0.0403/1.087	0.0296/1.226	0.0405/1.069
$R_1{}^a$ (all data)	0.0475	0.0334	0.0561
w$R_2{}^c$ [$I > 2\sigma(I)$]	0.1178	0.0704	0.0962
No. of param./restr.	1231/3	285/1	548/0
Residual density (e Å^{-3})	0.716	0.997	0.999

$^a R_1 = \Sigma||F_o| - |F_c||/\Sigma|F_o|$. ^{b} GOF $= \{\Sigma[w(F_o^2 - F_c^2)^2]/(n-p)\}^{1/2}$. ^{c} w$R_2 = [\Sigma[w(F_o^2 - F_c^2)^2]/\Sigma[w(F_o^2)^2]]^{1/2}$. Where $w = 1/[\sigma^2(F_o^2) + (aP)^2 + bP]$, $P = (F_o^2 + 2F_c^2)/3$.

CCD diffractometer equipped with a Mo-target rotating-anode X-ray source and a graphite monochromator (Mo-Kα, λ = 0.71073 Å). Final cell constants were obtained from least squares fits of all measured reflections. Structures were readily solved by Patterson method and subsequent difference Fourier techniques. The crystallographic data were listed in Table 1. ShelX97[9] was used for the structure solution and refinement. All non-hydrogen atoms were refined anisotropically. Hydrogen atoms were placed at the calculated positions and refined as riding atoms with isotropic displacement parameters. The toluene molecules of **1**·2toluene are heavily disordered and refined isotropically. The CO molecule and Br atom of $\mathbf{4}^+I_3^-$ are disordered with respect to the C_2 axis or the mirror plane bisecting the PQ ligand. The structure has been refined considering 12% of the Br atom on the CO (88%) site and 12% CO molecule on the Br (88%) site. In the ORTEP plot (Fig. 4) the disordered CO molecule and Br atom were deleted for clarity.

Density functional theory (DFT) calculations

All calculations reported in this article were done with the Gaussian 03W[10] program package supported by GaussView 4.1. The DFT[11] and TD DFT[12] calculations were performed at the level of Becke three parameter hybrid functional with the non-local correlation functional of Lee-Yang-Parr (B3LYP).[13] Gas-phase geometries of **1**, **2**, $\mathbf{1}_{Me}$, $\mathbf{2}_{Me}$ and $\mathbf{4}_{Me}{}^+$ with the singlet spin state were optimized† using Pulay's Direct Inversion[14] in the Iterative Subspace (DIIS), 'tight' convergent SCF procedure[15] ignoring symmetry. Similarly, gas-phase geometries of $\mathbf{3}_{Me}$, $\mathbf{1}_{Me}{}^+$, $\mathbf{1}_{Me}{}^-$, $\mathbf{2}_{Me}{}^+$, $\mathbf{2}_{Me}{}^-$ and $\mathbf{3}_{Me}{}^+$ were optimized† with doublet spin state. Frequencies of molecular bond vibrations were calculated on $\mathbf{1}_{Me}$ and $\mathbf{4}_{Me}{}^+$. In all calculations, a LANL2DZ basis set along with the corresponding effective core potential (ECP) was used for ruthenium and osmium metals.[16–18] Valence double zeta basis set, 6-31G[19] for H was used. For C, O, P and Cl non-hydrogen atoms valence double zeta with diffuse and polarization functions, 6-31++G**[20] as a basis set was employed for all calculations. The percentage contributions of metal, chloride and PQ ligand to the frontier orbitals were calculated using the GaussSum program package.[21] The sixty lowest singlet excitation energies on each of the optimized geometries of $\mathbf{1}_{Me}$, $\mathbf{2}_{Me}$, $\mathbf{1}_{Me}{}^+$, $\mathbf{1}_{Me}{}^-$, and $\mathbf{4}_{Me}{}^+$ were calculated by TD DFT method.[22] The nature of transitions were calculated by adding the probability of the same type among alpha and beta molecular orbitals.

Results and discussion

Syntheses and characterization

The paramagnetic and diamagnetic 9,10-phenanthrenequinone (PQ) complexes of ruthenium, osmium and rhodium isolated in this work are listed in Chart 2. Complexes **1** and **2** were prepared by the PPh_3 displacement reactions. Reaction of PQ with $[Ru^{II}(PPh_3)_3Cl_2]$ in toluene at 298 K affords dark green **1**. Similarly, the reaction of PQ with $[Os^{II}(PPh_3)_3Br_2]$ affords **2**.

trans-$[Ru(PQ)(PPh_3)_2Cl_2]$	s = 0	**1**
trans-$[Os(PQ)(PPh_3)_2Br_2]$	s = 0	**2**
cis-$[Rh(PQ)(PPh_3)_2Cl_2]$	s = 1/2	**3**
trans-$[Os(PQ)(PPh_3)_2(CO)Br]^+I_3^-$	s = 0	$\mathbf{4}^+I_3^-$

Chart 2 Isolated PQ complexes of ruthenium, osmium and rhodium ions (*cis* and *trans* isomers with respect to PPh_3 ligands).

Reaction of $RhCl_3{\cdot}3H_2O$ with PQ in the presence of three-fold excess of PPh_3 in boiling ethanol generates **3**. **1**, **2** and **3** were isolated in good yields. **4** was prepared by the reported procedure[4] and the diffusion of iodine in *n*-hexane to **4** in CH_2Cl_2 produces $\mathbf{4}^+I_3^-$ in lower yields.

Magnetic susceptibility measurements at 298 K have confirmed that **3** is one-electron paramagnetic while **1**, **2** and $\mathbf{4}^+$ are diamagnetic. The symmetric and anti-symmetric $\nu_{C=O}$ of the PQ ligand are significant to analyse the electronic state of the PQ ligand in these complexes. The IR spectral features of **1–3** complexes are similar to those of one-electron paramagnetic *trans*-$[M^{II}(PQ^{\cdot-})(PPh_3)_2(CO)(X)]$ and *cis*-$[M^{II}(PQ^{\cdot-})(PPh_3)(CO)(X)]$ (M = Ru, Os; X = Cl, Br) complexes.[4] In **1–3**, $\nu_{C=O}$ appears at 1482–1434 cm^{-1} prompting the existence of reduced $PQ^{\cdot-}$ ligand in all three complexes. On the contrary, in $\mathbf{4}^+I_3^-$, it appears at 1594 (s, $\nu_{c=o(asym)}$) and 1560 (m, $\nu_{C=O\,(sym)}$) cm^{-1} correlating the existence of the neutral PQ chelate. The frequencies of the molecular bond vibrations were calculated on $\mathbf{4}^+$ at the B3LYP/DFT level of theory and the data are used to assign the IR spectra of **1–3** and $\mathbf{4}^+I_3^-$ complexes. The required data are summarized in the experimental section. The $\nu_{C\equiv O}$ of $\mathbf{4}^+I_3^-$ at 1955 cm^{-1} is expectedly higher than that of **4** at 1909 cm^{-1} containing the $PQ^{\cdot-}$ ligand. The trans geometries of **1** and **2** were confirmed by the single crystal X-ray structure determinations while the cis geometry of **3** has been predicted by the features of UV-vis/NIR absorption spectra, EPR spectra and redox activities. However, the single crystal X-ray structure determination authenticated the trans geometry of $\mathbf{4}^+I_3^-$ in the crystals.

The UV-vis/NIR spectral data are summarized in Table 2. The spectra of **1–3** are shown in panel (a) of Fig. 1. The electronic absorption spectral features of **1** and **2** are very similar having characteristic strong NIR absorption bands at around 700 nm. The absorption band above 600 nm is absent in **3**. The absorption feature of **3** is similar to those of the paramagnetic *cis*-$[M^{II}(PQ^{\cdot-})(PPh_3)_2(CO)(X)]$ (M = Ru, Os; X = Cl, Br) complexes[4] as shown in panel (b) of Fig. 1. It corresponds to the *cis*-geometry of **3** incorporating a t_{2g}^{6} metal ion and the $PQ^{\cdot-}$ anion radical. However, the UV-vis/NIR absorption spectrum of the oxidized non-radical $\mathbf{4}^+I_3^-$ analogue is different (panel (c) of Fig. 1) and it does not display any lower energy absorption band. The origins of these spectral features were investigated by TD DFT calculations on the model $\mathbf{1}_{Me}$, $\mathbf{2}_{Me}$, $\mathbf{1}_{Me}^+$, $\mathbf{1}_{Me}^-$, and $\mathbf{4}_{Me}^+$ complexes. The results are discussed in the electronic absorption spectra section (*vide infra*).

Table 2 Electronic absorption spectra of **1–3** and $\mathbf{4}^+I_3^-$ in CH_2Cl_2 at 298 K

Complexes	λ_{max}/nm (ε, $10^4\ M^{-1}\ cm^{-1}$)
1	703 (1.56), 542 (0.69), 387 (1.46)
2	716 (1.04), 477 (0.36), 466 (0.48), 401 (0.69), 328 (1.08)
3	559 (0.26), 502 (0.38), 462 (0.35), 423 (0.38), 406 (0.48)
$\mathbf{4}^+I_3^-$	607 (0.22), 495 (0.33), 364 (1.53)

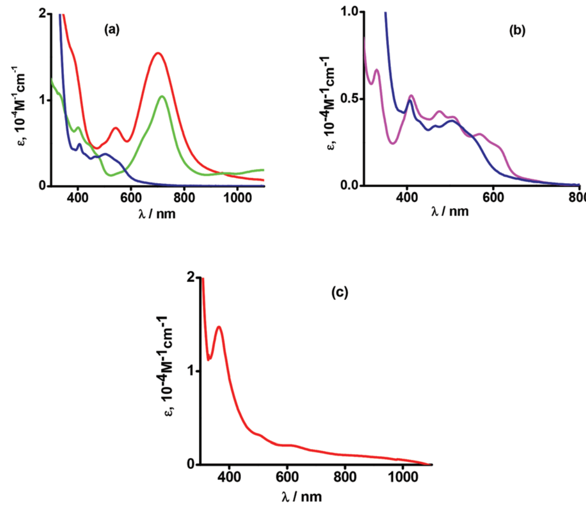

Fig. 1 UV-vis/NIR spectra of (a) **1** (red), **2** (green), **3** (blue) (b) *cis*-$[Ru^{II}(PQ^{\cdot-})(PPh_3)_2(CO)(Cl)]$ (magenta) *vs.* **3** (blue) and (c) $\mathbf{4}^+I_3^-$ in CH_2Cl_2 at 298 K.

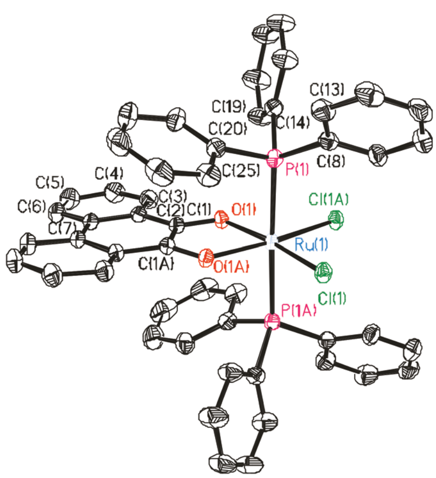

Fig. 2 ORTEP plot of **1**·2toluene with 40% thermal ellipsoids (toluene molecules and H atoms are omitted for clarity).

Single crystal X-ray structures

The molecular geometry of **1** has been confirmed by the single crystal X-ray structure determination of **1**·2toluene. It crystallizes in the *C*2/*c* space group. The molecular geometry and atom labelling scheme are shown in Fig. 2. Table 3 summarizes the selected bond parameters. The *trans*-$[RuO_2P_2Cl_2]$ octahedron is distorted. The OO-bite is only 78.6°. It is observed that the Ru–O and Ru–P lengths of **1**·2toluene deviate significantly from those of *trans*/*cis*-$[M^{II}(PQ^{\cdot-})(PPh_3)_2(CO)(X)]$ (M = Ru, Os; X = Cl, Br) complexes.[4] The average Ru–O lengths (σ bonding), 2.032(2) Å, of **1**·2toluene are comparatively shorter, while the average Ru–P lengths (π bonding), 2.418(2) Å, are comparatively longer. This length trend is consistent with the higher valence state of the ruthenium ion and the question is which one, Ru^{III} or Ru^{IV}, is present in **1**·2toluene?

The C–C and C–O bond lengths of the PQ-chelate neither support the di-keto (C–O and C–C lengths, 1.25 ± 1 and 1.45 ± 1 Å) nor the di-olato (C–O and C–C lengths, 1.35 ± 1 and 1.38 ± 1 Å) forms of the PQ as shown by **E** and **C** of Scheme 2.[4,3q]

Table 3 Selected experimental bond lengths (Å) and angles (°) of **1**·2toluene and corresponding parameters from CSS and BS DFT calculations on **1** and [Ru(PQ)(PMe$_3$)$_2$Cl$_2$] (**1**$_{Me}$), open shell solutions of **1**$_{Me}$$^+$ and **1**$_{Me}$$^-$

	Exp	Calc				
		Closed shell singlet solutions (CSS)		BS (1,1), M_s = 0	Open shell solutions (OSS)	
	1·2toluene	**1**	**1**$_{Me}$	**1**$_{Me}$	**1**$_{Me}$$^+$	**1**$_{Me}$$^-$
Ru(1)–O(1)	2.032(2)	2.078	2.053	2.102	2.103	2.082
Ru(1)–P(1)	2.418(2)	2.469	2.417	2.423	2.460	2.392
Ru(1)–Cl(1)	2.357(2)	2.436	2.461	2.382	2.340	2.496
O(1)–C(1)	1.286(4)	1.274	1.283	1.295	1.262	1.312
C(1)–C(1A)	1.415(7)	1.453	1.440	1.428	1.483	1.413
O(1)–Ru(1)–O(1A)	78.6(2)	76.26	77.30	76.93	73.92	79.34
Cl(1)–Ru(1)–Cl(1A)	96.2(1)	95.97	99.00	99.62	101.24	95.87
P(1)–Ru(1)–P(1A)	177.7(2)	171.31	160.65	175.39	169.52	172.71

In **1**·2toluene, the C–C length is 1.418(5) Å and the average C–O lengths are 1.291(3) Å. These bond parameters of the OO-chelate are comparable to those of *trans*/*cis*-[M^{II}(PQ$^{\cdot-}$)(PPh$_3$)$_2$(CO)(X)] (M = Ru, Os; X = Cl, Br) complexes prompting the existence of the PQ$^{\cdot-}$ anion radical in **1**·2toluene. This trend of bond parameters is consistent with the coordination of the paramagnetic PQ$^{\cdot-}$ to the paramagnetic ruthenium(III) ion as illustrated by the resonance form **D** of Scheme 2. DFT calculations (*vide infra*) on *trans*-[Ru(PQ)(PMe$_3$)$_2$Cl$_2$] (**1**$_{Me}$) confirmed that BS (1,1) S = 0 solution with the electronic state **D**, is more stable than the closed shell singlet (CSS) solutions with electronic states **C** and **E**.

Single crystal X-ray structure of **2**·CH$_2$Cl$_2$ confirmed the trans geometry and bond parameters of **2**. **2**·CH$_2$Cl$_2$ crystallizes in a centro-symmetric space group, *C*2/*c*. Molecular geometry with the atom labelling scheme is illustrated in Fig. 3. Bond parameters are listed in Table 4. The Os(1)–O(1) and Os(1)–Br(50) lengths are comparatively shorter than the corresponding Os–O and Os–Br lengths of *cis*-[Os^{II}(PQ$^{\cdot-}$)(PPh$_3$)$_2$(CO)Br][4] while the corresponding Os(1)–P(1) and Os(1)–P(2) lengths are comparatively longer. The features do not correlate with the coordination of PQ to the Os(II) ion, rather it favours the Os(III) state. The average C–O and C–C lengths of the OO-chelate respectively are 1.303(3) and 1.426(5) Å which correlate with the existence of the PQ$^{\cdot-}$ anion radical in **2**·CH$_2$Cl$_2$. The length trend suggests the coordination of PQ$^{\cdot-}$ to osmium(III) ion in **2**·CH$_2$Cl$_2$.

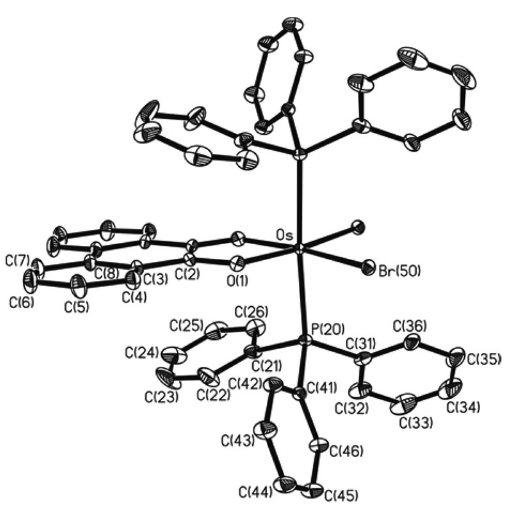

Fig. 3 ORTEP plot of **2**·CH$_2$Cl$_2$ with 40% thermal ellipsoids (CH$_2$Cl$_2$ molecule and H atoms are omitted for clarity).

4$^+$I$_3$$^-$ crystallizes in the *P*2$_1$/*c* space group. The molecular geometry and the atom labeling scheme are shown in Fig. 4. Bond parameters are summarized in Table 5. The trend of the bond parameters of the OO-chelate of **4**$^+$ is different from those of **1**·2toluene and **2**·CH$_2$Cl$_2$. The C–O lengths are comparatively shorter and the C–C length is longer (Table 5). It is consistent with the PQ chelation.[4,3q] The **4**$^+$ ion is an osmium(II) complex of the PQ ligand incorporating the resonance structure **E** of Scheme 2. The bond parameters of the coordination sphere and OO chelate of **4**$^+$ are significant to elucidate the electronic structures of **1**–**3** complexes. The average Os^{II}–O lengths are comparatively higher than those of Os^{III}–O lengths in **2**·CH$_2$Cl$_2$ complex (Tables 4 and 5). The Os–P lengths are shorter correlating the higher extent of Os^{II}-PPh$_3$ π-back bonding in **4**$^+$ ion.

Table 4 Experimental bond lengths (Å) and angles (°) of **2**·CH$_2$Cl$_2$ and calculated parameters of **2** and *trans*-[Os(PQ)(PMe$_3$)$_2$Br$_2$] (**2**$_{Me}$)

	Exp	Calc		
		Closed shell singlet solutions (CSS)		BS (1,1), M_s = 0
	2·CH$_2$Cl$_2$	**2**	**2**$_{Me}$	**2**$_{Me}$
Os(1)–O(1)	1.999(2)	2.040	2.039	2.039
Os(1)–P(1)	2.410(1)	2.462	2.420	2.420
Os(1)–Br(1)	2.525(0)	2.584	2.562	2.562
O(1)–C(1)	1.303(3)	1.303	1.306	1.306
C(1)–C(1A)	1.426(5)	1.420	1.419	1.419
O(1)–Os(1)–O(1A)	78.1(1)	76.96	77.48	77.48
Br(1)–Os(1)–Br(1A)	101.4(0)	95.44	97.89	97.89
P(1)–Os(1)–P(1A)	176.1(1)	173.98	172.5	172.5

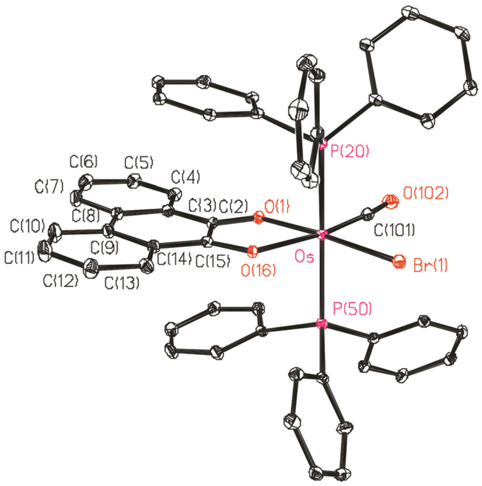

Fig. 4 ORTEP plot of $4^+I_3^-$ with 40% thermal ellipsoids (I_3^- and H atoms are omitted for clarity).

Table 5 Experimental bond lengths (Å) and angles (°) of $4^+I_3^-$ and calculated parameters of *trans*-[Os(PQ)$(PMe_3)_2$(CO)Br]$^+$ ($\mathbf{4}_{Me}^+$)

	Exp $\mathbf{4}^+I_3^-$	Calc $\mathbf{4}_{Me}^+$
Os–O(1)	2.140(3)	2.051
Os–O(16)	2.026(3)	2.183
Os–P(20)	2.398(1)	2.450
Os–P(50)	2.399(1)	2.448
Os–Br(1)	2.524(1)	2.566
Os(1)–C(101)	1.851(6)	1.855
O(1)–C(2)	1.266(5)	1.269
O(16)–C(15)	1.268(4)	1.279
C(2)–C(15)	1.466(6)	1.465
O(1)–Os–O(16)	75.8(1)	74.1
Br(1)–Os–C(101)	93.7(1)	94.4
P(20)–Os–P(50)	175.5(0)	168.4

EPR spectra

Magnetic susceptibilities measurements at 298 K confirmed the one electron paramagnetism of **3** (μ_{eff} = 1.77μ_B). **1** and **2** are diamagnetic. X-band EPR spectra of solid (83 K), solution (298 K) and frozen CH_2Cl_2 glasses (83 K) of **3** were recorded and spectra are illustrated in Fig. 5. The EPR parameters are summarized in Table S1.† The isotropic fluid solution EPR spectrum of **3** as depicted in panel (a) of Fig. 5 was simulated considering hyperfine couplings due to two *cis*-^{31}P (A/G, 9.1), ^{103}Rh (A/G, 1.7) and ^{31,37}Cl (A/G, 1.4) nuclei at g = 1.999. The g parameter correlates well with the presence of $PQ^{\cdot-}$ coordinated to rhodium(III), a low spin t_{2g} ion. However, the solid and frozen glass anisotropic EPR spectra as illustrated in panels (b) and (c) of Fig. 5 infer a minor contribution of the resonance form, **E** (Scheme 2) incorporating the rhodium(II), a $t_{2g}^6e_g^1$ ion coordinated to the neutral PQ ligand. Simulation of the solid state spectrum provides the g-parameters at $g_{11} = g_{22}$ = 2.001 and g_{33} = 1.987. The frozen glass spectrum was simulated at $g_{11} = g_{22}$ = 2.005 and g_{33} = 1.987 with the hyperfine couplings due to two ^{31}P ($A_{11} = A_{22}$/G, 10.0 and A_{33}/G, 11.17).

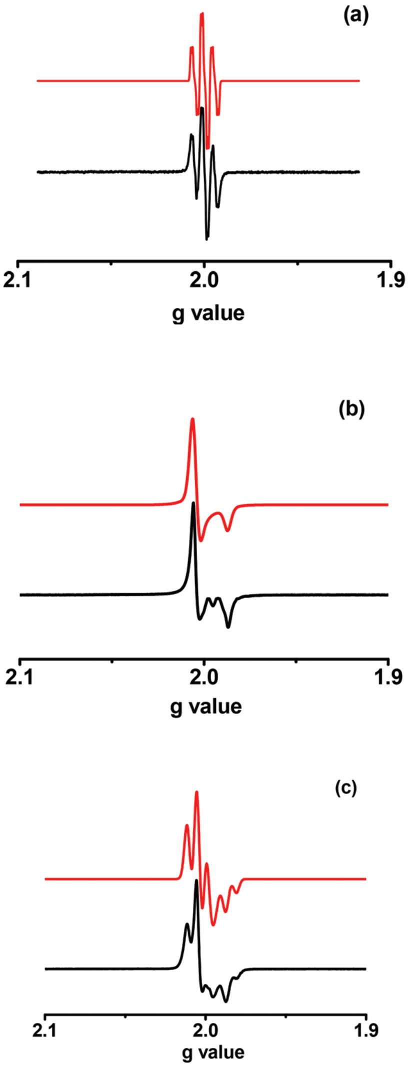

Fig. 5 X-band EPR spectra of (a) CH_2Cl_2 solution at 298 K (b) solid at 83 K and (c) CH_2Cl_2 frozen glass at 83 K of **3** (black = experimental spectra; red = simulated spectra).

The anisotropicity ($\Delta g = g_{max} - g_{min}$) in solid and glass is 0.018. The anisotropic parameter discloses a minor contribution of the resonance form **E**, [M^{II}(PQ)$(PPh_3)_2X_2$], to the ground electronic state of the [M(PQ)$(PPh_3)_2X_2$] complexes. These EPR parameters decline the existence of a Rh^{IV} ion, a metal centered radical coordinated to a diamagnetic dianionic 9,10-phenanthrenediolato (PQ^{2-}) ligand. The EPR spectral features are consistent with the coordination of the $PQ^{\cdot-}$ to M(III) metal ions in **1**–**3** as predicted by the X-ray structural bond parameters of **1**·2toluene and **2**·CH_2Cl_2 complexes.

Existence of the $PQ^{\cdot-}$ anion radical coordinated to the ruthenium(III) ion was also authenticated by the frozen glass EPR spectrum of the electrogenerated (*vide infra*) $\mathbf{1}^-$ which displays distinct signals due to both valence tautomers, *trans*-[Ru^{III}(PQ^{2-})$(PPh_3)_2Cl_2$]$^-$ and *trans*-[Ru^{II}($PQ^{\cdot-}$)$(PPh_3)_2Cl_2$]$^-$ (Table S1†). The EPR spectrum of $\mathbf{1}^-$ is illustrated in Fig. 6. Simulation established the two components of the spectrum.

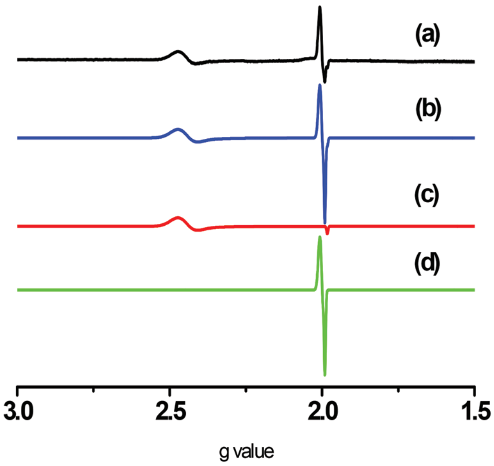

Fig. 6 X-band EPR spectra of CH_2Cl_2 frozen glass of **1**$^-$ at 83 K (black (a) = experimental spectra; blue (b) = simulated spectra considering the components of 0.3740 × *trans*-$[Ru^{III}(PQ^2)(PPh_3)_2Cl_2]^-$ + 3.740 × *trans*-$[Ru^{II}(PQ^{\cdot-})(PPh_3)_2Cl_2]^-$; red (c) = simulated spectrum of the pure component, 0.3740 × *trans*-$[Ru^{III}(PQ^{2-})(PPh_3)_2Cl_2]^-$; green (d) = simulated spectrum of the pure component, 3.740 × *trans*-$[Ru^{II}(PQ^{\cdot-})(PPh_3)_2Cl_2]^-$.

The major component is the axial spectrum with the *g*-parameters, $g_1 = g_2 = 2.456$; $g_3 = 1.983$. These parameters are due to a ruthenium(III) complex, *trans*-$[Ru^{III}(PQ^{2-})(PPh_3)_2X_2]^-$ incorporating a reduced di-olato ligand. While the minor component is an isotropic spectrum with $g_{iso} = 1.999$ correlating well with the existence of the $PQ^{\cdot-}$ anion radical coordinated to the ruthenium(II) ion as in *trans*-$[Ru^{II}(PQ^{\cdot-})(PPh_3)_2X_2]^-$. It is one of the significant observations that conclusively establish the electronic state of complexes **1**–**3**. However, no temperature dependent thermodynamic equilibrium between these two tautomers has been detected. Moreover, the ruthenium(III) signal is not detectable at room temperature.

Redox series

The redox activities of complexes **1**–**3** were investigated at 298 K by cyclic voltammetric experiments in CH_2Cl_2. The cyclic voltammograms are illustrated in Fig. 7 and the redox potential data referenced *vs.* ferrocenium/ferrocene, Fc^+/Fc, couple are summarized in Table S2.† The potentials of electro-activities of **1** and **2** are similar and metal independent. It infers that all the electron transfers are ligand centered. The features of redox waves are comparable to those of the *trans*-$[M(PQ^{\cdot-})(PPh_3)_2(CO)(X)]$ (M = Ru, Os; X = Cl, Br) family[4] but anodic potentials are shifted by +0.2–0.25 V and may be due to the higher oxidation state of the coordinated metal ion. It was established that the anodic and cathodic waves of the *trans*-$[M^{II}(PQ^{\cdot-})(PPh_3)_2(CO)(X)]$ analogues are reversible while the cathodic waves of the *cis*-$[M^{II}(PQ^{\cdot-})(PPh_3)_2(CO)(X)]$ analogues are irreversible due to PPh_3 dissociation. The reversibility of both the cathodic and anodic waves of **1** and **2** in CH_2Cl_2 are consistent with the trans geometries of complexes **1** and **2** in solution.

On the contrary, the cathodic wave of **3** in CH_2Cl_2 is irreversible as depicted by the voltammogram (i) of the panel

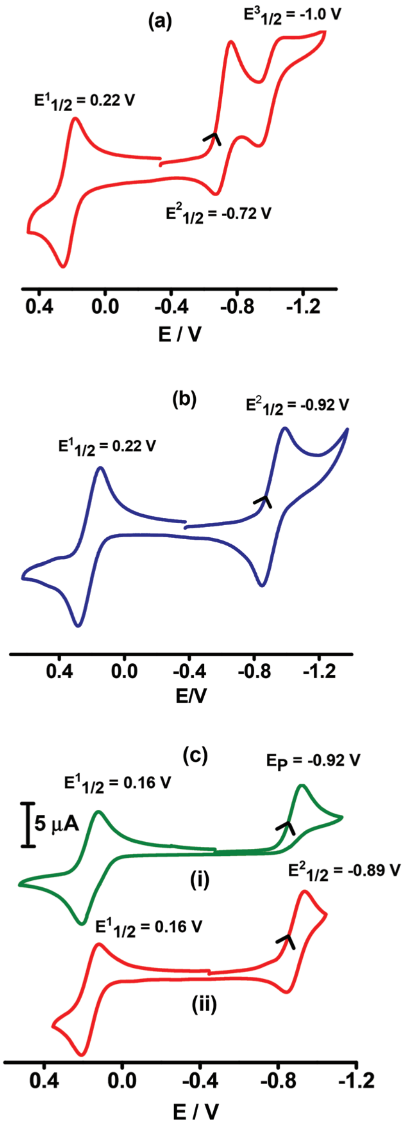

Fig. 7 Cyclic voltammograms of (a) **1** (b) **2** (c) **3** [panel (i)] in CH_2Cl_2 and (c) **3** in 0.025 mM PPh_3 solution of CH_2Cl_2 [panel (ii)] at 298 K. Conditions: 0.20 M $[N(n\text{-}Bu)_4]PF_6$ supporting electrolyte; platinum working electrode.

(c) of Fig. 7. The feature compares well with that of *cis*-$[M^{II}(PQ^{\cdot-})(PPh_3)_2(CO)(X)]$ complexes predicting a *cis*-geometry of **3**. Upon bulk electrolysis of **3** at −0.75 V at 298 K and analyses of the electrolyzed solution by ESI (+ve and −ve) mass spectra, detected the $[Rh(PQ)(PPh_3)X_2]^+$ ion other than PF_6^- and $[N(n\text{-}Bu)_4]^+$ ions. It infers that elimination of PPh_3 is one of the paths of dissociation of **3** upon reduction. The analogy of PPh_3 dissociation has been authenticated by reproducing a reversible cathodic wave of **3** in 0.25 mM PPh_3 solution of CH_2Cl_2 as illustrated by the voltammogram (ii) of the panel (c) of Fig. 7.

The metal independent redox potentials ($E^2_{1/2}$, Table S2† and Fig. 7) at +0.22, +0.22 and +0.16 V of **1**–**3** have been assigned to the $PQ/PQ^{\cdot-}$ redox couple. While the redox waves ($E^2_{1/2}$, Table S2†) at −0.72, −0.92 and −0.92 V are assigned to the $PQ^{\cdot-}/PQ^{2-}$ reduction couple. No other anodic waves assignable to the metal oxidation were detected in the

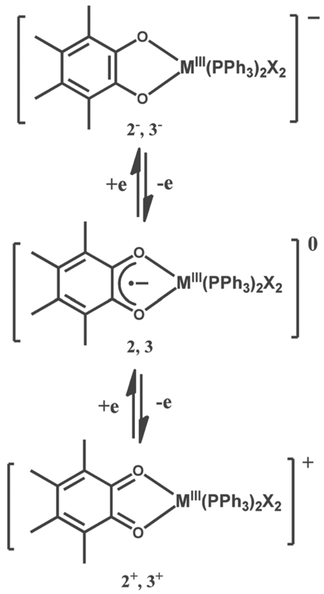

Scheme 3 Redox series of **2** (M = Os, X = Br) and **3** (M = Rh, X = Cl) complexes (PQ ligand is drawn schematically for clarity).

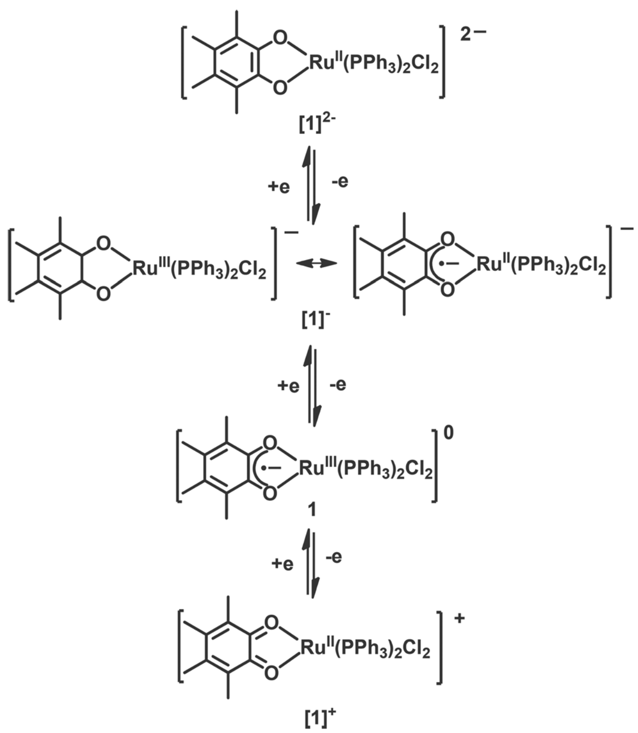

Scheme 4 Redox series of **1** (PQ ligand is drawn schematically for clarity).

experimental range (range: +2.0 to −2.0 V). The redox series of **2** and **3** are depicted in Scheme 3. However, an overlapping cathodic wave due to the Ru^{III}/Ru^{II} reduction couple ($E^3_{1/2}$) at −1.0 V has been detected in the case of **1**. Coulometric reduction of **1** by one-electron affords ligand reduction as well as metal reduced anions as *trans*-$[Ru^{III}(PQ^{2-})(PPh_3)_2Cl_2]^-$ and *trans*-$[Ru^{II}(PQ^{\bullet -})(PPh_3)_2Cl_2]^-$ which were detected by the frozen glass EPR spectrum of $\mathbf{1}^-$ (Fig. 6). The electronic state of $\mathbf{1}^-$ is thus defined by two valence tautomers and the redox series are illustrated in Scheme 4. DFT calculations (*vide infra*) also elucidated the spin density due to the ruthenium(III) ion and $PQ^{\bullet -}$ chelate in $\mathbf{1}^-$, which are elaborated below.

Electronic structures

Broken symmetry (BS) DFT calculations

$PQ^{\bullet -}$ coordination to ruthenium(III) and osmium(III) ions in ***1*** *and* ***2***. Gas-phase geometries of **1**, **2** (Fig. S1),† *trans*-$[Ru(PQ)(PMe_3)_2Cl_2]$ ($\mathbf{1}_{Me}$) and *trans*-$[Os(PQ)(PMe_3)_2Br_2]$ ($\mathbf{2}_{Me}$) were optimized using the singlet spin state at the B3LYP level of theory. The calculated parameters of **1** and $\mathbf{1}_{Me}$ are listed in Table 3. The calculated parameters of **2** and $\mathbf{2}_{Me}$ are summarized in Table 4. Surprisingly, it is observed that the closed shell singlet (CSS) solutions of **1**, **2**, $\mathbf{1}_{Me}$ and $\mathbf{2}_{Me}$ are unstable due to open shell singlet (OSS) perturbations, *i.e.*, neutral PQ coordination to Ru(II) or Os(II) ions are unstable. The molecular orbitals of the restricted CSS solution of $\mathbf{1}_{Me}$ are depicted in Fig. 8 which shows that HOMO−2, one of the molecular orbitals of the t_{2g} set has a strong interaction with the π^*_{PQ} and is composed of 46% π^*_{PQ} and 39% d_{Ru}. The shifting of d-electrons to the PQ ligand by the HOMO−2 is a concern in elucidating the electronic structure of $\mathbf{1}_{Me}$. A similar feature is observed in the case of $\mathbf{2}_{Me}$ (Fig. 8).

Stability analysis of the singlet self-consistent field (SCF) solution has established that the CSS solution of $\mathbf{1}_{Me}$ is unstable with respect to OSS perturbations as the lowest Hessian eigenvalue is negative (−0.0088) due to HOMO−2 to LUMO excitations. Surprisingly, LUMO is composed of 63%

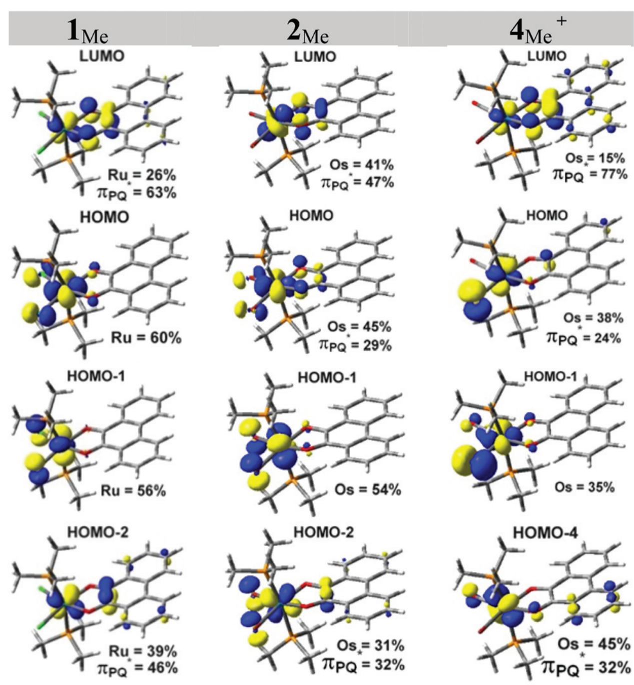

Fig. 8 Significant molecular orbitals obtained from the closed shell singlet solutions of $\mathbf{1}_{Me}$, $\mathbf{2}_{Me}$ and $\mathbf{4}_{Me}^+$.

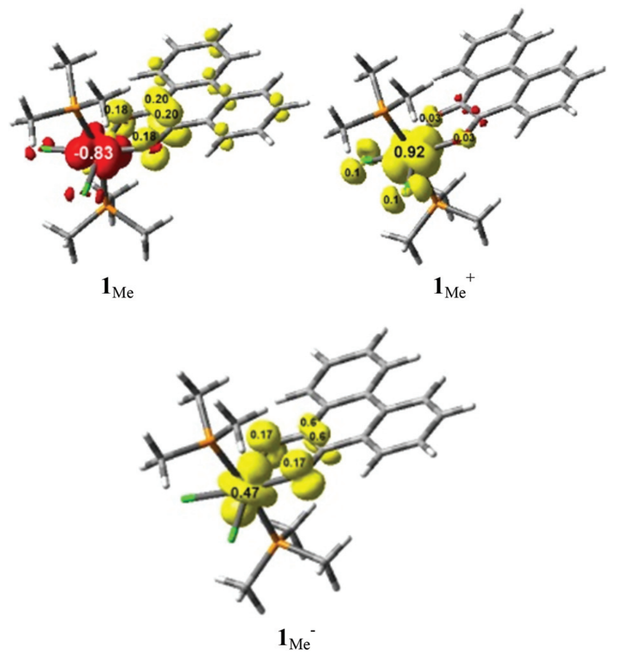

Fig. 9 Spin density distribution in $\mathbf{1}_{Me}$ obtained from BS (1,1) M_s = 0 DFT calculations and spin densities of $\mathbf{1}_{Me}^+$ and $\mathbf{1}_{Me}^-$ ions. Values of atomic spin densities obtained from Mulliken spin population analyses.

π^*_{PQ} ligand and 26% d_{Ru} orbital. The negative lowest eigenvalue of excitation in $\mathbf{1}_{Me}$ contradicts the CSS as a stable ground state of $\mathbf{1}_{Me}$ and implies that the lowest energy wave function is due to a singlet di-radical that requires an unrestricted BS solution for proper descriptions.

Re-optimization of the unstable CSS solution of $\mathbf{1}_{Me}$ using the BS DFT method leads to a stable di-radical singlet defined as BS (1,1) M_s = 0 solution. The state is described by two fragments and the notation BS (1,1) refers to a broken symmetry state with 1 unpaired spin-up electron on PQ fragment transforming $PQ^{\cdot-}$ and 1 unpaired spin-down electron essentially localized on the Ru(III) center. The spin density distribution of BS (1,1) M_s = 0 solutions of $\mathbf{1}_{Me}$ are illustrated in Fig. 9. It shows the localization of spin density predominantly on ruthenium center and the PQ ligand affirming the presence of reduced PQ ligand, *i.e.*, $PQ^{\cdot-}$ coordinated to one electron paramagnetic ruthenium(III) ion in $\mathbf{1}_{Me}$ as in the resonance form **D** of Scheme 2. $\mathbf{1}_{Me}$ is defined as *trans*-[$Ru^{III}(PQ^{\cdot-})(PPh_3)_2Cl_2$]. Bond parameters of the BS (1,1) M_s = 0 and CSS solutions of $\mathbf{1}_{Me}$ are summarized in Table 3 for comparison. Bond parameters of both the solutions are comparable but the BS (1,1) M_s = 0 solution of $\mathbf{1}_{Me}$ is 22.6 kJ mole^{-1} lower in energy than the corresponding CSS solutions.

Similarly, the CSS solution of $\mathbf{2}_{Me}$ is unstable. Mixing of the d_{Os} orbital with the π* orbital of the PQ (HOMO–2, Fig. 8) results in the transfer of the electron from the osmium ion to the PQ ligand and destabilizes the osmium(II) state in $\mathbf{2}_{Me}$. BS (1,1) M_s = 0 solution is stable establishing the di-radical state of $\mathbf{2}_{Me}$ as *trans*-[$Os^{III}(PQ^{\cdot-})(PPh_3)_2Br_2$]. The BS (1,1) M_s = 0 solution is 24.2 kJ mol^{-1} lower in energy than the CSS

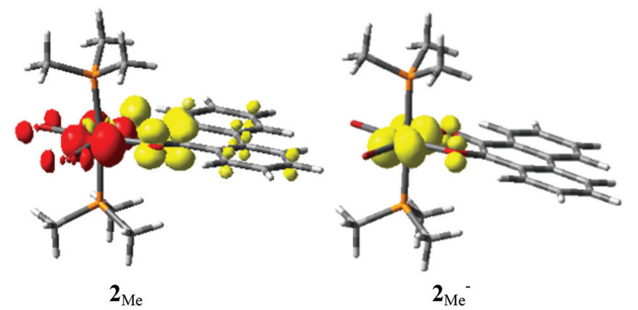

Fig. 10 Spin density distribution in $\mathbf{2}_{Me}$ obtained from BS (1,1) M_s = 0 DFT calculations (b) $\mathbf{2}_{Me}^-$. Values of atomic spin densities obtained from Mulliken spin population analyses: $\mathbf{2}_{Me}$; O1, +0.16; C1, +0.15; C2, +0.15; O2, +0.16; C4, +0.05; C6, +0.06; C11, +0.05, C13, +0.06; Os, −0.62. $\mathbf{2}_{Me}^-$; O1, +0.06; O2, +0.06; Os, +0.83.

solution. Spin density localization on the osmium ion and the PQ ligand as illustrated in Fig. 10 authenticated the di-radical description of $\mathbf{2}_{Me}$. Bond parameters of the CSS and BS (1,1) M_s = 0 solutions of $\mathbf{2}_{Me}$ are summarized in Table 4 for comparison.

On the contrary, no mixing of the π^*_{PQ} with the d_{Os} was observed in the $\mathbf{4}_{Me}^+$ ion. The LUMO is composed of 77% π^*_{PQ} and 15% d_{Os}. The three t_{2g} orbitals do not have any component of the π^*_{PQ} orbital. No CSS-open shell singlet (OSS) perturbation is observed and the CSS solution of $\mathbf{4}_{Me}^+$ is stable.

Coordination of $PQ^{\cdot-}$ to rhodium(III) in **3**. Ground state electronic structure of **3** was elucidated by unrestricted density functional theory (DFT) calculation on $\mathbf{3}_{Me}$.

Gas phase geometry of $\mathbf{3}_{Me}$ was optimized with the doublet spin state and the calculated geometrical parameters are summarized in Table 6. The calculated longer C–O and comparatively shorter C–C lengths of the OO-chelate are consistent with the existence of the $PQ^{\cdot-}$ chelate (resonance form **D** of Scheme 2) in **3**. Because of cis geometry, Rh–O(1) and Rh–O(2), Rh–P(1) and Rh–P(2), Rh–Cl(1) and Rh–Cl(2) lengths are different as listed in Table 6.

Mulliken spin density analyses reveal that the spin density is predominantly localized on the PQ chelate reducing PQ to $PQ^{\cdot-}$ as shown in Fig. 11. The isotropic EPR spectrum at 298 K with g = 1.999 is consistent with this description. The spin density is predominantly localized on the α-HOMO which is composed of 88% PQ ligand and 8% rhodium d-orbital. It is to be noted that the spin density is localized equally over

Table 6 Calculated bond lengths (Å) and angles (°) of $\mathbf{3}_{Me}$, $\mathbf{3}_{Me}^+$ and $\mathbf{3}_{Me}^-$

	$\mathbf{3}_{Me}$	$\mathbf{3}_{Me}^+$	$\mathbf{3}_{Me}^-$
Rh–O(1)	2.085	2.140	2.050
Rh–O(2)	2.155	2.240	2.098
Rh–P(1)	2.352	2.369	2.322
Rh–P(2)	2.314	2.308	2.329
Rh–Cl(1)	2.433	2.433	2.470
Rh–Cl(2)	2.399	2.350	2.471
O(1)–C(1)	1.299	1.254	1.348
O(2)–C(2)	1.287	1.245	1.334
C(2)–C(1)	1.438	1.525	1.393

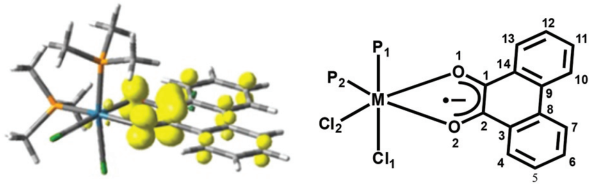

Fig. 11 Spin density distribution in 3_{Me}. Values of atomic spin densities obtained from the Mulliken spin population analyses: O1, 0.18; C1, 0.24; C2, 0.24; O2, 0.18; C4, 0.08; C6, 0.08; C11, 0.08, C13, 0.08; Rh, 0.04.

carbon and oxygen atoms explaining well the comparatively longer C–O and shorter C–C lengths of the OO-chelate. The calculated spin density on the rhodium ion is less than 5%. It infers a minor contribution of the resonance form, *trans*-[Rh^{II}(PQ)(PPh_3)$_2$$Cl_2$] incorporating a metallo radical as shown by **E** of the Scheme 2. The contribution of **E** was justified by anisotropic EPR spectra (Table S1† and Fig. 5) of the solid and CH_2Cl_2 frozen glasses of **3** at 83 K.

Neutral PQ chelation to osmium(II) ion in 4$^+$. To elucidate the electronic structure of 4^+ ion, the gas-phase geometry of the *trans*-[Os(PQ)(PMe_3)$_2$(CO)(Br)]$^+$ ($4_{Me}{}^+$) ion was optimized using a singlet spin state. Analysis of the stability confirms that the CSS solution of the $4_{Me}{}^+$ ion is stable inferring the coordination of the PQ to the osmium(II) ion. The calculated bond parameters are summarized in Table 5. The calculated bond lengths are comparable to those found in the single crystal X-ray structure determination of $4^+I_3{}^-$. The shorter C–O and the comparatively longer C–C lengths of the PQ chelate are consistent with the neutral PQ chelation to the osmium(II) ion incorporating pure structure **E** of Scheme 2. Thus, considering the IR spectra, calculated experimental bond parameters and the stability of the solution, the 4^+ ion is defined as a PQ complex of osmium(II) as in *trans*-[Os^{II}(PQ)(PPh_3)$_2$(CO)Br]$^+$.

Neutral PQ chelation to M(III) ion in [1–3]$^+$

trans-[Ru^{III}(PQ)(PPh$_3$)$_2$Cl$_2$]$^+$ (1$^+$), trans-[Os^{III}(PQ)(PPh$_3$)$_2$Br$_2$]$^+$ (2$^+$) and trans-[Rh^{III}(PQ)(PPh$_3$)$_2$Cl$_2$]$^+$ (3$^+$). The origin of the metal independent reversible redox waves ($E^1_{1/2}$) of **1**, **2** and **3** at +0.22, +0.22 and +0.16 V is also a subject of investigation. DFT calculations elucidated that the reversible electron transfer event is due to the PQ/PQ$^{\cdot-}$ redox couple. The electronic structures of 1^+, 2^+ and 3^+ were analyzed by unrestricted DFT calculations on $1_{Me}{}^+$ and $2_{Me}{}^+$ using doublet spin state and restricted DFT calculations on $3_{Me}{}^+$ using singlet spin state. The bond parameters of the optimized geometries of $1_{Me}{}^+$ and $2_{Me}{}^+$ are listed respectively in Tables 3 and 4. The bond parameters of the optimized geometry of $3_{Me}{}^+$ are listed in Table 6. In all cases, comparatively two shorter C–O and a longer C–C lengths of the OO-chelate are consistent with the neutral PQ description as observed in $4^+I_3{}^-$, *trans*-[Ru^{II}(PQ)(PPh_3)$_2$(CO)Cl]$^+I_3{}^-$ and [Cu(dppf)(PQ)]BF_4 complexes.[4,3q] Spin density obtained from the Mulliken spin population analyses of $1_{Me}{}^+$ and $2_{Me}{}^+$ are mainly localized on the ruthenium and osmium ion as shown in Fig. 9 confirming the ruthenium(III) and osmium(III) states. The $3_{Me}{}^+$ ion is diamagnetic. However, calculations on $3_{Me}{}^+$ using singlet spin state revealed a similar trend of bond lengths as observed in $1_{Me}{}^+$ and $1_{Me}{}^+$ assuring the ligand oxidation. Thus, the [**1–3**]$^+$ complexes are defined as *trans*-[M^{III}(PQ)(PPh_3)$_2$$X_2$]$^+$. The complexes [**1–3**]$^+$ are the hitherto unknown examples of the neutral PQ chelation to ruthenium(III), osmium(III) and rhodium(III) ions.

Di-anionic PQ^{2-} chelation to M(III) ions in [2–3]$^-$. The reduction wave of **2** at the cathode is reversible while the wave is irreversible in the case of **3** due to PPh_3 dissociation. In the presence of 0.025 mM PPh_3, the reduction wave is reversible (Fig. 7). The reduction potential data of **2** and **3** are metal independent. It occurs respectively at −0.92 and 0.89 V. The electronic structures of 2^- and 3^- were investigated by DFT calculations on $2_{Me}{}^-$ and $3_{Me}{}^-$ using doublet and singlet spin states, respectively. The calculated bond parameters are summarized in Tables 4 and 6. The length trend of the OO-chelate is the reverse to those found upon oxidation. Comparatively, longer C–O and shorter C–C bond lengths of the OO-chelate infer the presence of the reduced di-anionic PQ^{2-} ligand in $2_{Me}{}^-$ and $3_{Me}{}^-$. Thus, the electron transfer events of **2** and **3** at −0.92 and −0.89 V referenced *vs.* Fc^{+}/Fc couple has been defined as the reduction of the PQ$^{\cdot-}$ to the di-anionic PQ^{2-} ligand and the anions 2^- and 3^- are respectively defined as *trans*-[Os^{III}(PQ^{2-})(PPh_3)$_2$$Cl_2$]$^-$ and *cis*-[Rh^{III}(PQ^{2-})(PPh_3)$_2$$Cl_2$]$^-$. The spin density plot as shown in Fig. 10 confirms the existence of Os(III) in $2_{Me}{}^-$ ion. No spin density localization on the PQ ligand is noted in $2_{Me}{}^-$. It is consistent with the cyclic voltammogram of **2**. On the contrary, spin density in 1^- is delocalized over both the metal and PQ ligand inferring the existence of both the valence tautomers (*vide infra*).

Valence tautomers of 1$^-$

trans-[Ru^{III}(PQ^{2-})(PPh$_3$)$_2$Cl$_2$]$^-$ vs. trans-[Ru^{II}(PQ$^{\cdot-}$)(PPh$_3$)$_2$Cl$_2$]$^-$. EPR spectrum (Fig. 6) detected both the valence tautomers, [Ru^{III}(PQ^{2-})(PPh_3)$_2$$Cl_2$] ↔ [Ru^{II}(PQ$^{\cdot-}$)($PPh_3$)$_2$$Cl_2$], in 1^-. DFT calculation with the doublet spin state authenticated that the spin density of $1_{Me}{}^-$ is delocalized over both the ruthenium ion and OO-chelate equally as depicted in Fig. 9 correlating the presence of both Ru$^{II/III}$ electromers in 1^- as shown in Scheme 4. In $1_{Me}{}^-$, the average oxidation state of the ruthenium ion is 2.5, while the average oxidation state of the PQ ligand is −1.5 defining the 1^- ion as *trans*-[Ru$^{2.5}$(PQ$^{1.5-}$)-(PPh_3)$_2$$Cl_2$]$^-$. The calculated bond parameters are listed in Table 3. The average C–O length, 1.311 Å, is higher than that of PQ$^{\cdot-}$ (1.290 Å, Tables 3, 4 and 6) and lower than that of PQ^{2-} (Table 6, 1.341 Å) ligands. The corresponding C–C lengths (1.413 Å) of the OO-chelate is shorter than that in a PQ$^{\cdot-}$ (1.436 Å) and higher than that in a PQ^{2-} (1.400 Å) ligand. Thus, the redox state of the PQ ligand in $1_{Me}{}^-$ has been defined as an intermediate between PQ$^{\cdot-}$ and PQ^{2-} states justifying the spin density distribution and the EPR spectrum of the 1^- ion. Thus the cathodic wave of **1** at −0.72 V has been assigned to the reduction of Ru^{III} to Ru^{II} (50%) and PQ$^{\cdot-}$ to PQ^{2-} ligand (50%).

Electronic absorption spectra of 1 and 2

Closed shell singlet (CSS)-open shell singlet (OSS) perturbation MLCT. The electronic absorption spectra of **1** and **2** are conspicuous. The absorption band of **1** and **2** at 700 nm which is

Table 7 Excitation energies (*λ*, nm), oscillator strengths (*f*), transition types and dominant contributions of charge transfer bands of **1**, $\mathbf{1}^+$, $\mathbf{1}^-$, **2** and $\mathbf{4}^+$ obtained from TD DFT calculations on $\mathbf{1}_{Me}$, $\mathbf{1}_{Me}{}^+$, $\mathbf{1}_{Me}{}^-$, $\mathbf{2}_{Me}$ and $\mathbf{4}_{Me}{}^+$

Calc *λ*/nm	*f*	Exp *λ*	Significant contributions (>10%)	Transition types	Dominant contributions
$\mathbf{1}_{Me}$ (experimental data correspond to **1**)					
643.6	0.302	701	HOMO–3 → LUMO (22%)	$p_P(43) + p_{Cl}(53) \rightarrow d_{Ru}(26) + \pi_L^*(63)$	ILCT
			HOMO–2 → LUMO (54%)	$d_{Ru}(39) + \pi_L(46) \rightarrow d_{Ru}(26) + \pi_L^*(63)$	CSS–OSS MLCT
597.2	0.147	543	HOMO–3 → LUMO (72%)	$p_P(43) + p_{Cl}(53) \rightarrow d_{Ru}(26) + \pi_L^*(63)$	ILCT
			HOMO–2 → LUMO (13%)	$d_{Ru}(39) + \pi_L(46) \rightarrow d_{Ru}(26) + \pi_L^*(63)$	CSS–OSS MLCT
381.6	0.033	383	HOMO–8 → LUMO (88%)	$d_{Ru}(13) + p_{Cl}(70) \rightarrow d_{Ru}(26) + \pi_L^*(63)$	MMLLCT
314.0	0.135		HOMO–1 → LUMO + 2 (86%)	$d_{Ru}(56) + p_{Cl}(37) \rightarrow \pi_L^*(99)$	MLCT
307.1	0.113		HOMO–2 → LUMO + 2 (85%)	$d_{Ru}(39) + \pi_L(46) \rightarrow \pi_L^*(99)$	MMLLCT
305.4	0.065		HOMO–13 → LUMO (74%)	$\pi_L(99) \rightarrow d_{Ru}(26) + \pi_L(63)$	LLCT
$\mathbf{1}_{Me}{}^+$ (experimental data correspond to the electrogenerated $\mathbf{1}^+$ ion)					
587.4	0.278		αHOMO–3 → LUMO (51%)	$d_{Ru}(47) + \pi_L(25) + p_{Cl}(20) \rightarrow \pi_L^*(89)$	MMLLCT
			βHOMO–2 → LUMO (23%)	$d_{Ru}(40) + \pi_L(30) + p_P(29) \rightarrow d_{Ru}(13) + \pi_L^*(82)$	MMLMMLCT
423.6	0.042		αHOMO–6 → LUMO (38%)	$\pi_L(94) \rightarrow \pi_L(89)$	LLCT
			βHOMO–5 → LUMO (49%)	$\pi_L(93) \rightarrow d_{Ru}(13) + \pi_L(82)$	LMMLCT
389.8	0.033		βHOMO–6 → LUMO + 1 (86%)	$d_{Ru}(14) + \pi_L(18) + p_{Cl}(66) \rightarrow d_{Ru}(70) + p_{Cl}(24)$	MMLMMLCT
323.8	0.040		βHOMO → LUMO + 1 (78%)	$d_{Ru}(53) + p_{Cl}(39) \rightarrow d_{Ru}(70) + p_{Cl}(24)$	d–d Transition
$\mathbf{1}_{Me}{}^-$ (experimental data correspond to the electrogenerated $\mathbf{1}^-$ ion)					
861.8	0.122		βHOMO–2 → LUMO (83%)	$d_{Ru}(51) + \pi_L(29) + p_{Cl}(18) \rightarrow d_{Ru}(38) + \pi_L^*(55)$	MMLMMLCT
357.9	0.031		αHOMO–2 → LUMO + 1 (24%)	$d_{Ru}(62) + p_{Cl}(29) \rightarrow \pi_L^*(99)$	MLCT
			αHOMO → LUMO + 4 (32%)	$d_{Ru}(14) + \pi_L(81) \rightarrow d_{Ru}(62) + p_P(38)$	MMLMCT
			βHOMO–1 → LUMO + 2 (23%)	$d_{Ru}(64) + p_{Cl}(24) \rightarrow \pi_L^*(99)$	MLCT
334.3	0.045		αHOMO–3 → LUMO (25%)	$d_{Ru}(36) + \pi_L(14) + p_{Cl}(44) \rightarrow \pi_L^*(100)$	MMLLCT
			αHOMO → LUMO + 7 (11%)	$d_{Ru}(14) + \pi_L(81) \rightarrow \pi_L^*(93)$	MMLLCT
			βHOMO → LUMO + 8 (26%)	$d_{Ru}(55) + \pi_L(27) + p_{Cl}(17) \rightarrow \pi_L^*(74) + p_P(25)$	MMLLCT
			βHOMO → LUMO + 9 (11%)	$d_{Ru}(55) + \pi_L(27) + p_{Cl}(17) \rightarrow \pi_L^*(78) + p_P(17)$	MMLLCT
$\mathbf{2}_{Me}$ (experimental data correspond to **2**)					
705.3	0.137	716	HOMO–4 → LUMO (13%)	$\pi_L(14) + p_P(45) + p_{Br}(32) \rightarrow d_{Os}(41) + \pi_L(47) + p_{Br}(10)$	LMMLCT
			HOMO–2 → LUMO (61%)	$d_{Os}(31) + \pi_L(32) + p_{Br}(30) \rightarrow d_{Os}(41) + \pi_L^*(47) + p_{Br}(10)$	MMLMMLCT
330.0	0.042	410	HOMO–2 → LUMO + 1 (11%)	$d_{Os}(31) + \pi_L(32) + p_{Br}(30) \rightarrow \pi_L^*(99)$	MMLLCT
			HOMO–1 → LUMO + 2 (23%)	$d_{Os}(54) + p_{Br}(36) \rightarrow \pi_L^*(97)$	MLCT
			HOMO–1 → LUMO + 3 (30%)	$d_{Os}(54) + p_{Br}(36) \rightarrow d_{Os}(58) + \pi_L^*(14) + p_{Br}(27)$	MMMLCT
			HOMO → LUMO + 4 (16%)	$d_{Os}(45) + \pi_L(29) + p_{Br}(25) \rightarrow \pi_L^*(23) + p_P(49)$	MMLLCT
314.0	0.037	328	HOMO–2 → LUMO + 2 (74%)	$d_{Os}(31) + \pi_L(32) + p_{Br}(30) \rightarrow \pi_L^*(97)$	MMLLCT
$\mathbf{4}_{Me}{}^+$ (experimental data correspond to $\mathbf{4}^+I_3{}^-$)					
794.9	0.085		HOMO–3 → LUMO (10%)	$d_{Os}(15) + \pi_L(20) + p_P(41) + p_{Br}(24) \rightarrow d_{Os}(15) + \pi_L^*(77)$	MMLMMLCT
			HOMO → LUMO (61%)	$d_{Os}(38) + \pi_L(24) + p_{Br}(35) \rightarrow d_{Os}(15) + \pi_L^*(77)$	MMLMMLCT
552.0	0.125	607	HOMO–4 → LUMO (12%)	$d_{Os}(45) + \pi_L(32) + \pi_{CO}(11) \rightarrow d_{Os}(15) + \pi_L^*(77)$	MMLMMLCT
			HOMO–3 → LUMO (70%)	$d_{Os}(15) + \pi_L(20) + p_P(41) + p_{Br}(24) \rightarrow d_{Os}(15) + \pi_L^*(77)$	MMLMMLCT
528.5	0.149	495	HOMO–4 → LUMO (69%)	$d_{Os}(45) + \pi_L(32) + \pi_{CO}(11) \rightarrow d_{Os}(15) + \pi_L^*(77)$	MMLMMLCT
416.0	0.037	364	HOMO–6 → LUMO (83%)	$d_{Os}(16) + \pi_L(73) \rightarrow d_{Os}(15) + \pi_L^*(77)$	MMLMMLCT
310.6	0.099		HOMO → LUMO + 1 (91%)	$d_{Os}(38) + \pi_L(24) + p_{Cl}(35) \rightarrow \pi_L^*(99)$	MMLLCT

MLCT = metal to ligand charge transfer; ILCT = inter ligand charge transfer; LLCT = ligand to ligand charge transfer; MMLMMLCT = mixed metal ligand to mixed metal ligand charge transfer; MMMLCT = metal to mixed metal ligand charge transfer; LMMLCT = ligand to mixed metal ligand charge transfer; MMLMCT = mixed metal ligand to metal charge transfer; MMLLCT = mixed metal ligand to ligand charge transfer; CSS-OSS MLCT = closed shell singlet-open shell singlet MLCT

absent in **3** (Fig. 1), carries the information of the instability of the CSS solutions of **1** and **2**. The origin of the lower energy absorption bands has been elucidated by TD DFT calculations on $\mathbf{1}_{Me}$ and $\mathbf{2}_{Me}$ with the singlet spin state. Excitation energies of the transitions with oscillator strengths greater than 0.03, are summarized in Table 7. Analyses of the calculations of $\mathbf{1}_{Me}$ authenticated that the transition from HOMO–2 (Ru, 39% + PQ, 46%) to LUMO (Ru, 26% + PQ, 63%) are responsible for the CSS to OSS perturbation with the negative Hessian eigenvalue, is a major component of this low energy absorption band (see, Table 7). The transition has thus been assigned to the transfer of electrons from the d_{Ru} orbital (HOMO–2) to the π_{PQ}^* (LUMO) and is defined as a CSS–OSS perturbation MLCT. The changes of features of CSS–OSS perturbation MLCT upon one electron oxidation or reduction of **1** in CH_2Cl_2 at 298 K were recorded by spectro-electrochemical and coulometric experiments and are illustrated in Fig. 12. The CSS–OSS perturbation MLCT is absent in $[\mathbf{1}–\mathbf{4}]^+$, $[\mathbf{1}–\mathbf{4}]^-$ and **3**. The lower energy absorption bands of **1** and **2** at 700 nm disappear in $\mathbf{1}^+$ and $\mathbf{2}^+$ ions and a new absorption band at 600 nm (panels (a) and (b) of Fig. 12) due to MLCT (Table 7) appears in both complexes.

Upon reduction, the intensities of these absorption bands of **1** and **2** decrease as illustrated in panels (c) and (d) of Fig. 12. This finding augments the knowhow of this MLCT as a CSS–OSS perturbation MLCT that does not depend much on the electronic states of the origin or source separately. The origin of this band thus has been assigned to the excitation of one of the paired electrons to occupy two different orbitals, one being the metal and another being the PQ ligand,

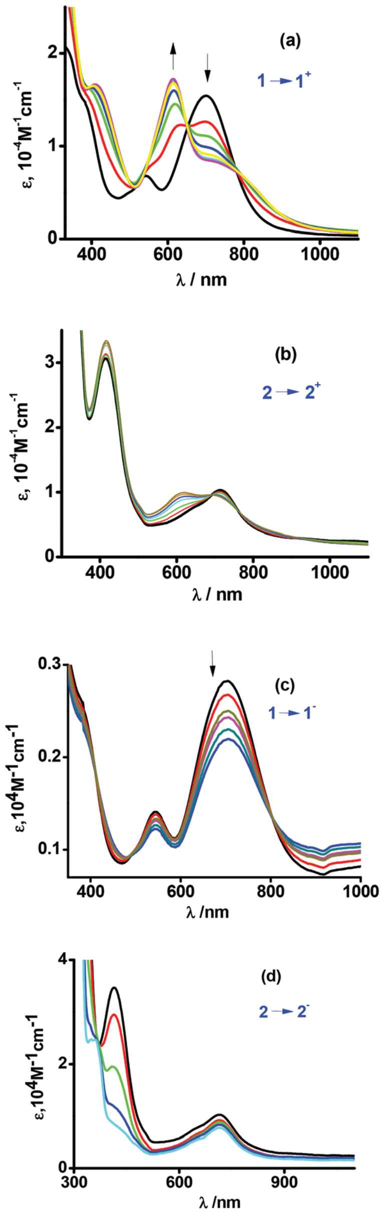

Fig. 12 Spectro-electrochemistry of **1** and **2** showing the electronic spectra of electrochemically generated (a) $\mathbf{1}^{+}$, (b) $\mathbf{2}^{+}$, (c) $\mathbf{1}^{-}$ and (b) $\mathbf{2}^{-}$ in CH_2Cl_2 at 298 K.

resulting in a singlet ground state. The absorption band is due to the conversion of CSS to OSS and is a hallmark to define the unstable CSS state.

The absorption features of **1**–**3** complexes at 400 nm are characteristic. TD DFT calculations on $\mathbf{1}_{\mathrm{Me}}$, $\mathbf{2}_{\mathrm{Me}}$ and $\mathbf{3}_{\mathrm{Me}}$ have elucidated that the origin of this absorption band as a transition to the singly occupied π^{*}_{PQ}. The finding corroborates well with the presence of the $\mathrm{PQ}^{\cdot-}$ anion radical in all three complexes. The effect of oxidation or reduction on this absorption band has been recorded by spectro-electrochemical measurements on **1** and **2**. It is noted that the intensity of absorption band at 410 nm expectedly increases upon oxidation and decreases upon reduction.

Conclusions

In this work, the electronic structures of the diamagnetic *trans*-[M(PQ)$(PPh_3)_2X_2$] [M = Ru, X = Cl, **1**; M = Os, X = Br, **2**] and paramagnetic *cis*-[Rh(PQ)$(PPh_3)_2Cl_2$] (**3**) complexes were authenticated as $\mathrm{PQ}^{\cdot-}$ complexes of ruthenium(III), osmium(III) and rhodium(III) as in *trans*/*cis*-[$\mathrm{M^{III}}(\mathrm{PQ}^{\cdot-})(PPh_3)_2X_2$]. A minor contribution of the *trans*/*cis*-[$\mathrm{M^{II}}$(PQ)$(PPh_3)_2X_2$] form was predicted by the anisotropic frozen glass EPR spectrum of **3**. The closed shell singlet (CSS) solutions of *trans*-[Ru(PQ)$(PMe_3)_2Cl_2$] ($\mathbf{1}_{\mathrm{Me}}$) and *trans*-[Os(PQ)$(PMe_3)_2Br_2$] ($\mathbf{2}_{\mathrm{Me}}$) are unstable due to open shell singlet (OSS) perturbation. However, BS (1,1) $M_s = 0$ solutions of $\mathbf{1}_{\mathrm{Me}}$ and $\mathbf{2}_{\mathrm{Me}}$ are lower in energies and reproduced the experimental bond parameters in good agreement. Similar to [$\mathrm{M^{II}}(\mathrm{PQ}^{\cdot-})(PPh_3)_2$(CO)X] complexes,[4] the redox series of *trans*/*cis*-[$\mathrm{M^{III}}(\mathrm{PQ}^{\cdot-})(PPh_3)_2X_2$] complexes are PQ centered and upon one-electron oxidation produce PQ complexes of type *trans*/*cis*-[$\mathrm{M^{III}}$(PQ)$(PPh_3)_2X_2]^{+}$. Reduction of **2** and **3** produces PQ^{2-} complexes of type *trans*/*cis*-[$\mathrm{M^{III}}(\mathrm{PQ}^{-2})(PPh_3)_2X_2$]. **1** displays two overlapping cathodic waves and, most significantly, both the valence tautomers, *trans*-[$\mathrm{Ru^{III}}(\mathrm{PQ}^{2-})(PPh_3)_2Cl_2]^{-}$ and *trans*-[$\mathrm{Ru^{II}}(\mathrm{PQ}^{\cdot-})(PPh_3)_2Cl_2]^{-}$, were detected by the frozen glass EPR spectrum of $\mathbf{1}^{-}$. It unequivocally confirms the coordination of $\mathrm{PQ}^{\cdot-}$ to M(III) ion in **1**–**3**. The study substantiated a new electronic spectral feature of the unstable CSS state which produce absorption bands at lower energy due to perturbation to OSS state. The strong absorption bands of **1** and **2** at 703 and 716 nm, respectively, are defined as CSS–OSS perturbation MLCT those are absent in stable singlet [**1**–**4**]$^{+}$ ions. The investigation discards the report of the coordination of the reducing PQ^{2-} to the oxidizing ruthenium(IV) ion in the [Ru(PQ)$(PPh_3)_2Cl_2$] complex.

Acknowledgements

Financial support received from DST (SR/S1/IC/0026/2012) and CSIR (3231/NS-EMRII) New Delhi, India is gratefully acknowledged. M. K. B is thankful to CSIR, New Delhi, India, for fellowship (8/531(0007)/2012-EMR-I).

Notes and references

1 J. Stubbe and W. A. van der Donk, *Chem. Rev.*, 1998, **98**, 705.

2 (*a*) A. Sokolowski, J. Müller, T. Weyhermüller, R. Schnepf, P. Hildebrandt, K. Hildenbrand, E. Bothe and K. Wieghardt, *J. Am. Chem. Soc.*, 1997, **119**, 8889; (*b*) Y. Wang, J. L. DuBois, B. Hedman, K. O. Hodgson and T. D. P. Stack, *Science*, 1998, **279**, 537; (*c*) P. Chaudhuri and K. Wieghardt, *Prog. Inorg. Chem.*, 2001, **50**, 151; (*d*) P. Chaudhuri, M. Hess, U. Flörke and K. Wieghardt, *Angew. Chem., Int. Ed.*, 1998, **37**, 2217; (*e*) B. T. Op't Holt, M. A. Vance, L. M. Mirica, D. E. Heppner, T. D. P. Stack and

E. I. Solomon, *J. Am. Chem. Soc.*, 2009, **131**, 6421; (*f*) D. P. Goldberg, S. P. Watton, A. Masschelein, L. Wimmer and S. J. Lippard, *J. Am. Chem. Soc.*, 1993, **115**, 5346; (*g*) D. P. Goldberg, D. Koulougliotis, G. W. Brudvig and S. J. Lippard, *J. Am. Chem. Soc.*, 1995, **117**, 3134; (*h*) R. C. Pratt and T. D. P. Stack, *J. Am. Chem. Soc.*, 2003, **125**, 8716; (*i*) T. Storr, P. Verma, R. C. Pratt, E. C. Wasinger, Y. Shimazaki and T. D. P. Stack, *J. Am. Chem. Soc.*, 2008, **130**, 15448; (*j*) J. A. Halfen, B. A. Jazdzewski, S. Mahapatra, L. M. Berreau, E. C. Wilkinson, L. Que Jr. and W. B. Tolman, *J. Am. Chem. Soc.*, 1997, **119**, 8217; (*k*) M. Foti, K. U. Ingold and J. Lusztyk, *J. Am. Chem. Soc.*, 1994, **116**, 9440; (*l*) L. Valgimigli, R. Amorati, M. GraziaFumo, G. A. DiLabio, G. F. Pedulli, K. U. Ingold and D. A. Pratt, *J. Org. Chem.*, 2008, **73**, 1830.

3 (*a*) P. Milko and J. Roithová, *Inorg. Chem.*, 2009, **48**, 11734; (*b*) G. Speier, S. Tisza, A. Rockenbauer, S. R. Boone and C. G. Pierpont, *Inorg. Chem.*, 1992, **31**, 1017; (*c*) C. G. Pierpont and H. H. Downs, *Inorg. Chem.*, 1977, **16**, 2970; (*d*) C. G. Pierpont and R. M. Buchanan, *J. Am. Chem. Soc.*, 1975, **97**, 6450; (*e*) C. G. Pierpont and R. M. Buchanan, *J. Am. Chem. Soc.*, 1975, **97**, 4912; (*f*) A. S. Batsanov, J. A. K. Howard, M. A. Brown, B. R. McGarvey and D. G. Tuck, *Chem. Commun.*, 1997, 699; (*g*) D. A. Hutchinson, K. S. Chen, J. Russell and J. K. S. Wan, *J. Chem. Phys.*, 1980, **73**, 1862; (*h*) M. Leirer, G. Knör and A. Vogler, *Z. Naturforsch., B: Chem. Sci.*, 1999, **54**, 1039; (*i*) P. J. Crowley and H. M. Haendler, *Inorg. Chem.*, 1962, **1**, 904; (*j*) M. Leirer, G. Knör and A. Vogler, *Z. Naturforsch., B: Chem. Sci.*, 1999, **54**, 1039; (*k*) K. Broadley, N. G. Connelly and W. E. Geiger, *J. Chem. Soc., Dalton Trans.*, 1983, 121; (*l*) S. R. Wang, C. P. Cheng and T.-I. Ho, *J. Chem. Soc., Dalton Trans.*, 1988, 2695; (*m*) T.-I. Ho, C.-M. Chang, S. R. Wang and C. P. Cheng, *J. Chem. Soc., Dalton Trans.*, 1988, 123; (*n*) E. K. Brechin, L. Calucci, U. Englert, L. Margheriti, G. Pampaloni, C. Pinzino and A. Prescimone, *Inorg. Chim. Acta*, 2008, **361**, 2375; (*o*) D. Weir and J. K. S. Wan, *J. Organomet. Chem.*, 1981, **220**, 323; (*p*) T. Foster, K. S. Chen and J. K. S. Wan, *J. Organomet. Chem.*, 1980, **184**, 113; (*q*) S. Roy, B. Sarkar, D. Bubrin, M. Niemeyer, S. Zli, G. K. Lahiri and W. Kaim, *J. Am. Chem. Soc.*, 2008, **130**, 15230; (*r*) W. Kaim, *Coord. Chem. Rev.*, 1987, **76**, 187; (*s*) C. Floriani, R. Henzi and F. Calderazzo, *J. Chem. Soc., Dalton Trans.*, 1972, 2640; (*t*) R. M. Ramadan, *J. Coord. Chem.*, 1997, **42**, 181; (*u*) A. L. Balch and Y. S. Sohn, *J. Organomet. Chem.*, 1971, **30**, C31; (*v*) O. Gandolfi, B. Giovannitti, M. Ghedini and G. Dolcetti, *J. Organomet. Chem.*, 1976, **104**, C41; (*w*) B. Giovannitti, O. Gandolfi, M. Ghedini and G. Dolcetti, *J. Organomet. Chem.*, 1977, **129**, 207.

4 M. K. Biswas, S. C. Patra, A. N. Maity, S.-C. Ke, N. D. Adhikary and P. Ghosh, *Inorg. Chem.*, 2012, **51**, 6687.

5 A. Y. Girgis, Y. S. Sohn and A. L. Balch, *Inorg. Chem.*, 1975, **14**, 2327.

6 (*a*) C. G. Pierpont and S. Kitagawa, Valence Tautomerism of Metal Complexes, in *Inorganic Chromotropism: Basic Concepts and Applications of Colored Materials*, ed. Y. Fukuda, Elsevier, Tokyo, 2007, p. 116; (*b*) D. N. Hendrickson and C. G. Pierpont, Valence Tautomeric Transition Metal Complexes, in *Topics in Current Chemistry*, ed. P. Gütlich and H. A. Goodwin, Springer-Verlag, Berlin, 2004, vol. 234, p. 63; (*c*) C. G. Pierpont, *Coord. Chem. Rev.*, 2001, **216–217**, 99; (*d*) G. Speier, Z. Tyeklár, P. Tóth, E. Speier, S. Tisza, A. Rockenbauer, A. M. Whalen, N. Alkire and C. G. Pierpont, *Inorg. Chem.*, 2001, **40**, 5653.

7 T. A. Stephenson and G. Wilkinson, *J. Inorg. Nucl. Chem.*, 1966, **28**, 945.

8 P. R. Hoffman and K. G. Caulton, *J. Am. Chem. Soc.*, 1975, **97**, 4221.

9 (*a*) G. M. Sheldrick, *ShelXS97*, Universität Göttingen, Germany, 1997; (*b*) G. M. Sheldrick, *ShelXL97*, Universität Göttingen, Germany, 1997.

10 M. J. Frisch, G. W. Trucks, H. B. Schlegel, G. E. Scuseria, M. A. Robb, J. R. Cheeseman Jr., J. A. Montgomery, T. Vreven, K. N. Kudin, J. C. Burant, J. M. Millam, S. S. Iyengar, J. Tomasi, V. Barone, B. Mennucci, M. Cossi, G. Scalmani, N. Rega, G. A. Petersson, H. Nakatsuji, M. Hada, M. Ehara, K. Toyota, R. Fukuda, J. Hasegawa, M. Ishida, T. Nakajima, Y. Honda, O. Kitao, H. Nakai, M. Klene, X. Li, J. E. Knox, H. P. Hratchian, J. B. Cross, R. Ammi, C. Pomelli, J. W. Ochterski, P. Y. Ayala, K. Morokuma, G. A. Voth, P. Salvador, J. J. Dannenberg, V. G. Zakrzewski, S. Dapprich, A. D. Daniels, M. C. Strain, O. Farkas, D. K. Malick, A. D. Rabuck, K. Raghavachari, J. B. Foresman, J. V. Ortiz, Q. Cui, A. G. Baboul, S. Clifford, J. Cioslowski, B. B. Stefanov, G. Liu, A. Liashenko, P. Piskorz, I. Komaromi, R. L. Martin, D. J. Fox, T. Keith, M. A. Al-Laham, C. Y. Peng, A. Nanayakkara, M. Challacombe, P. M. W. Gill, B. Johnson, W. Chen, M. W. Wong, C. Gonzalez and J. A. Pople, *GAUSSIAN 03 (Revision E.01)*, Gaussian, Inc., Wallingford, CT 06492, 2005.

11 (*a*) D. R. Salahub and M. C. Zerner, *The Challenge of d and f Electrons*, ACS, Washington, D.C., 1989; (*b*) R. G. Parr and W. Yang, *Density Functional Theory of atoms and molecules*, Oxford University Press, Oxford, U.K., 1989; (*c*) W. Kohn and L. Sham, *J. Phys. Rev.*, 1965, **140**, A1133; (*d*) P. Hohenberg and W. Kohn, *Phys. Rev.*, 1964, **136**, B864.

12 (*a*) R. E. Stratmann, G. E. Scuseria and M. Frisch, *J. Chem. Phys.*, 1998, **109**, 8218; (*b*) M. E. Casida, C. Jamoroski, K. C. Casida and D. R. Salahub, *J. Chem. Phys.*, 1998, **108**, 4439; (*c*) R. Bauernschmitt and R. Ahlrichs, *Chem. Phys. Lett.*, 1996, **256**, 454.

13 (*a*) A. D. Becke, *J. Chem. Phys.*, 1993, **98**, 5648; (*b*) B. Miehlich, A. Savin, H. Stoll and H. Preuss, *Chem. Phys. Lett.*, 1989, **157**, 200; (*c*) C. Lee, W. Yang and R. G. Parr, *Phys. Rev. B: Condens. Matter*, 1988, **37**, 785.

14 P. Pulay, *J. Comput. Chem.*, 1982, **3**, 556.

15 H. B. Schlegel and J. J. McDouall, in *Computational Advances in Organic Chemistry*, ed. C. Ogretir and I. G. Csizmadia, Kluwer Academic, The Netherlands, 1991, p. 167.

16 P. J. Hay and W. R. Wadt, *J. Chem. Phys.*, 1985, **82**, 270.
17 W. R. Wadt and P. J. Hay, *J. Chem. Phys.*, 1985, **82**, 284.
18 P. J. Hay and W. R. Wadt, *J. Chem. Phys.*, 1985, **82**, 299.
19 (*a*) V. A. Rassolov, M. A. Ratner, J. A. Pople, P. C. Redfern and L. A. Curtiss, *J. Comput. Chem.*, 2001, **22**, 976; (*b*) M. M. Francl, W. J. Pietro, W. J. Hehre, J. S. Binkley, D. J. DeFrees, J. A. Pople and M. S. Gordon, *J. Chem. Phys.*, 1982, **77**, 3654; (*c*) P. C. Hariharan and J. A. Pople, *Mol. Phys.*, 1974, **27**, 209; (*d*) P. C. Hariharan and J. A. Pople, *Theor. Chim. Acta*, 1973, **28**, 213; (*e*) W. J. Hehre, R. Ditchfield and J. A. Pople, *J. Chem. Phys.*, 1972, **56**, 2257.
20 T. Clark, J. Chandrasekhar, G. W. Spitznagel and P. V. R. Schleyer, *J. Comput. Chem.*, 1983, **4**, 294.
21 N. M. O'Boyle, A. L. Tenderholt and K. M. Langner, *J. Comput. Chem.*, 2008, **29**, 839.
22 (*a*) M. Cossi, N. Rega, G. Scalmani and V. Barone, *J. Comput. Chem.*, 2003, **24**, 669; (*b*) V. Barone and M. Cossi, *J. Phys. Chem. A*, 1998, **102**, 1995.